Graz University of Technology

MS Thesis

Mutual Interference in Automotive FMCW Radar

Modeling and Mitigation Techniques

conducted at the
Signal Processing and Speech Communication Laboratory
Graz University of Technology, Austria

in co-operation with
Infineon Technologies Austria AG
Graz, Austria

by
Mate Andras Toth, BSc.

Supervisors:
Assoc.Prof. Dipl.-Ing. Dr. Klaus Witrisal
Dipl.-Ing. Dr. Paul Meissner
Dipl.-Ing. Dr. Alexander Melzer

Assessor:
Assoc.Prof. Dipl.-Ing. Dr. Klaus Witrisal

Graz, June 20, 2018

Abstract

Radar sensors make use of reflections of electromagnetic waves to sense the surrounding environment. They are being increasingly utilized for automotive applications due to their flexibility and robustness with respect to environmental factors such as weather and ambient light conditions. In particular, radar is one of the key sensing technologies for ADAS (Advanced Driver Assistance Systems), as well as for autonomous driving technologies. In order to enable such safety-critical applications, very high requirements are placed on sensor performance. For an accurate and reliable detection of environmental objects, disturbance effects must be quantified and coped with.

With the rising number of radar-equipped vehicles on the roads, the issue of mutual interference arises. If multiple sensors are present within radar range and operate in the same radio frequency band, they possibly receive each others' transmitted signals. This results in a disturbance of the respective measurement, which can lead to a highly unreliable sensor performance. Mutual interference is predicted to become a very significant problem in the future; therefore, it is imperative to develop practical approaches for its quantification and mitigation.

Besides infrastructural measures to lower the probability of interference occurrence, signal processing algorithms play a key role in interference mitigation. The approach is to devise algorithms, to be implemented as part of the processing chain of the radar sensor, capable of processing the signals affected by interference. For the analysis as well as synthesis of such algorithms, a proper signal processing perspective on interference is needed, which is the topic of this thesis.

The work focuses on the prevalent signaling scheme used currently in automotive applications, FMCW (Frequency Modulate Continuous Wave)/CS (Chirp Sequence) radar. Novel results are presented concerning the exact modeling of the interference of two or more independently transmitting sensors. A simple but effective parametric description is used to derive an analytical expression for the frequency spectrum of the resulting interference signal. A statistical description in the context of the Range-Doppler processing of an interfered ramp sequence is given, as well. Furthermore, the model is experimentally verified, proving its validity.

The second key point of the work is a comprehensive treatise of mitigation methods. While not focusing on a single novel approach, the majority of state of the art methods is introduced and analyzed. In particular, performance metrics are defined, suitable for a general comparison of the different types of algorithms. These measures highlight the impact of interference on the detectability of objects as well as on further signal processing tasks such as angle estimation.

An accurate model enables a quantitative description of signal impairments caused by interference, and the performance comparison allows for a systematic evaluation of mitigation methods. Hence, a basis for further mitigation algorithm development is established, facilitating an analytical approach as opposed to heuristics.

Kurzfassung

Radarsensoren nutzen die Reflektionen von elektromagnetischen Wellen, um ihre Umgebung wahrzunehmen. Sie finden zunehmend Verwendung in Automobilanwendungen aufgrund ihrer Flexibilität und Robustheit bezüglich Umwelteinflüssen wie beispielweise Wetter und Beleuchtung. Radar ist insbesondere eine der Schlüsseltechnologien für ADAS (Advanced Driver Assistance Systems), sowie für autonomes Fahren. Um solche sicherheitskritische Anwendungen zu ermöglichen, werden sehr hohe Anforderungen an das Verhalten von Sensoren gestellt. Für eine genaue und zuverlässige Detektion von Umgebungsobjekten müssen Störeffekte quantifiziert und bewältigt werden.

Mit der steigenden Anzahl von mit Radarsensoren ausgestatteten Fahrzeugen auf den Straßen tritt das Problem der gegenseitigen Interferenz auf. Falls mehrere Sensoren sich innerhalb der Radarreichweite befinden und im gleichen Frequenzbereich senden, empfangen sie möglicherweise die gesendeten Signale voneinander. Dies hat eine Störung der jeweiligen Messung zur Folge, welche zu einem unzuverlässigen Sensorverhalten führen kann. Gegenseitige Interferenz wird in Zukunft zu einem sehr ernsthaften Problem; es ist also unerlässlich, geeignete Methoden für ihre Quantifizierung und Behandlung zu entwickeln.

Neben infrastrukturellen Maßnahmen zur Verringerung der Wahrscheinlichkeit von Interferenzereignissen spielen Signalverarbeitungsalgorithmen eine wichtige Rolle in der Behandlung von Interferenz. Als Teil der Verarbeitungskette des Sensors werden Algorithme benötigt, die fähig sind, mit Interferenz behafteten Signale zu verarbeiten. Für die Analyse sowie Synthese solcher Algorithmen ist eine angemessene Signalverarbeitungsperspektive der Interferenz notwendig, welche das Thema dieser Arbeit ist.

Schwerpunkt der Arbeit ist das für Automobilanwendungen derzeit meist verbreitete FM-CW (Frequency Modulated Continuous Wave)/CS (Chirp Sequence) Radar. Neue Resultate bezüglich der exakten Modellierung der Interferenz von zwei oder mehr unabhängig sendenden Sensoren werden vorgestellt. Eine simple, jedoch effektive parametrische Beschreibung wird verwendet, um einen analytischen Ausdruck für das Frequenzspektrum des entstandenen Interferenzsignals herzuleiten. Ebenso wird eine statistische Beschreibung der Range-Doppler Verarbeitung einer interferierten Rampensequenz vorgestellt. Zusätzlich wird das Modell experimentell verifiziert, wodurch seine Gültigkeit nachgewiesen wird.

Der zweite Hauptpunkt dieser Arbeit ist eine umfassende Abhandlung von Interferenzbehandlungsmethoden. Anstatt auf einen einzigen neuen Ansatz zu fokussieren wird der Großteil der Stand der Technik beschrieben und analysiert. Insbesondere werden Leistungsmaße definiert, die zu einem allgemeinen Vergleich von Algorithmen verschiedener Arten geeignet sind. Diese Maße heben den Einfluss von Interferenz auf das Detektionsvermögen von Objekten sowie auf die weiteren Verarbeitungsschritte, wie zum Beispiel Winkelschätzung, hervor.

Ein genaues Signalmodell liefert eine quantitative Beschreibung der von Interferenz versursachten Signalstörungen, und ein Vergleich durch Leistungsmaße ermöglicht eine systematische Auswertung von Behandlungsmethoden. Dadurch wird eine Basis für die Entwicklung weiterer Algorithmen aufgestellt, die einen analytischen Ansatz, im Gegensatz zu Heuristik, unterstützt.

Acknowledgement – Danke!

I had a pleasant experience over the past seven months being able to work on an interesting topic, for which I am truly grateful.

First of all, I would like to thank Klaus Witrisal for supervising my thesis. Klaus suggested me this project, gave invaluable insight in several crucial moments and was a great supervisor as a whole. I would like to thank him especially for placing trust in me as a student and for making sure that I get a fantastic supervision at Infineon Technologies, where I did my day-to-day work.

Speaking of which, I owe a huge thank you to my two colleagues, Paul Meissner and Alexander Melzer, for supervising me at the company. They are both not only extremely knowledgeable in the art and science of signal processing, but – maybe even more importantly – great people. In particular, thank you Alex for your contagious enthusiasm, and thank you Paul for your helpfulness and patience. I would like to also express my gratitude to my other colleagues, as well as to the company Infineon for having this possibility.

A special thank you goes to my friends and family. Thank you to the friends I worked (and laughed) with the whole time through university; I might not have made it without you guys. Finally, thanks to my parents for selflessly supporting me and my siblings for encouraging me; it is a privilege to have such a family.

Statutory Declaration

I declare that I have authored this thesis independently, that I have not used other than the declared sources/resources, and that I have explicitly marked all material which has been quoted either literally or by content from the used sources.

date	(signature)

Abbreviations

AAF	Anti-Aliasing Filter
ACC	Adaptive Cruise Control
ADAS	Advanced Driver Assistance Systems
ADC	Analog-to-Digital Converter
AR	AutoRegressive
AWGN	Additive White Gaussian Noise
BSD	Blind Spot Detection
CA	Cell Averaging
CDF	Cumulative Distribution Function
CFAR	Constant False Alarm Rate
CS	Chirp Sequence
DFT	Discrete Fourier Transform
DSP	Digital Signal Processor
ENBW	Equivalent Noise Bandwidth
EVM	Error Vector Magnitude
FE	Front End
FFT	Fast Fourier Transform
FMCW	Frequency Modulated Continuous Wave
IF	Intermediate Frequency
IFFT	Inverse FFT
IMAT	Iterative Method with Adaptive Thresholding
IVM	Instrumental Variable Method
MIMO	Multiple Input Multiple Output
NF	Noise Factor
RCS	Radar Cross Section
RD	Range-Doppler
RF	Radio Frequency
SINR	Signal-to-Interference-and-Noise Ratio
SNR	Signal-to-Noise Ratio
SSA	Singular Spectrum Analysis

Notational Conventions

j	imaginary unit
$\Re\{\}$	real part
$\Im\{\}$	imaginary part
$\{a, b\}$	set of a, b
$\boldsymbol{M}$	matrix notation (bold and uppercase)
$(R \times C)$	matrix dimensions (R rows and C columns)
$\boldsymbol{M}^{\mathrm{T}}$	matrix (or vector) transpose
$\boldsymbol{v}$	(column) vector notation (bold and lowercase)
u	scalar u
$\hat{x}$	estimate of x
$s\,(t)$	continuous-time signal

$S(f)$	signal in frequency-domain
$s[n]$	sampled signal
$\tilde{s}[n]$	signal after (mitigation) processing
$s^{(m)}[n]$	range-doppler matrix interpreted as a two-dimensional signal (column m, row n)
$\mathrm{P}(x)$	probability of x
	Subscripts
a_{I}	subscript indicates a pertaining to interfering sensor transmit signal
a_{V}	subscript indicates a pertaining to victim sensor transmit signal
a_{O}	subscript indicates a pertaining to object
a_{int}	subscript indicates a pertaining to interference component of received signal
a_{IF}	subscript indicates a pertaining to intermediate frequency
a_{IQ}	subscript indicates a pertaining to I/Q receiver

Frequently Used Symbols

A	signal amplitude
B_{IF}	intermediate frequency bandwidth
$B_{\{\mathrm{I,V}\}}$	interferer/victim ramp bandwidth
c	speed of light
d	measured radial distance (range)
f_0	start frequency
k	slope of frequency ramp
n	generic *fast-time* sample index (row of Range-Doppler matrix)
M	number of ramps in a measurement cycle (i.e., size of a row of the non-zero-padded RD matrix)
m	generic *slow-time* sample index (column of Range-Doppler matrix)
N	number of received samples per ramp (i.e., size of a column of the non-zero-padded RD matrix)
P_{int}	power (of interference received by victim sensor)
T_{int}	duration (of interference burst)
$T_{\{\mathrm{I,V}\}}$	interferer/victim ramp duration
v	measured relative radial velocity
φ	time-domain signal phase
ϕ	phase course in frequency domain
τ_{O}	time delay of object reflection
τ_{int}	point in time (of interference burst)

Contents

1 Introduction

1.1 Fundamentals and Motivation

Automotive radar has evolved from initial experimental setups in the 1970s, to the first commercial comfort system for high-end cars in the late 1990s, to an essential element of a modern vehicle's safety features [1]. In particular, radar plays an important role for ADAS (Advanced Driver Assistance Systems) applications and is crucial for future *autonomous driving* technologies [2]. The market penetration of radar sensors has experienced rapid growth and is expected to continue to do so in the future [3].

Figure 1.1 illustrates that a modern vehicle may be equipped with radar sensors in several locations. Sensors of different beamwidths and ranges can be used for different ADAS such as BSD (Blind Spot Detection), ACC (Adaptive Cruise Control) and others [4].

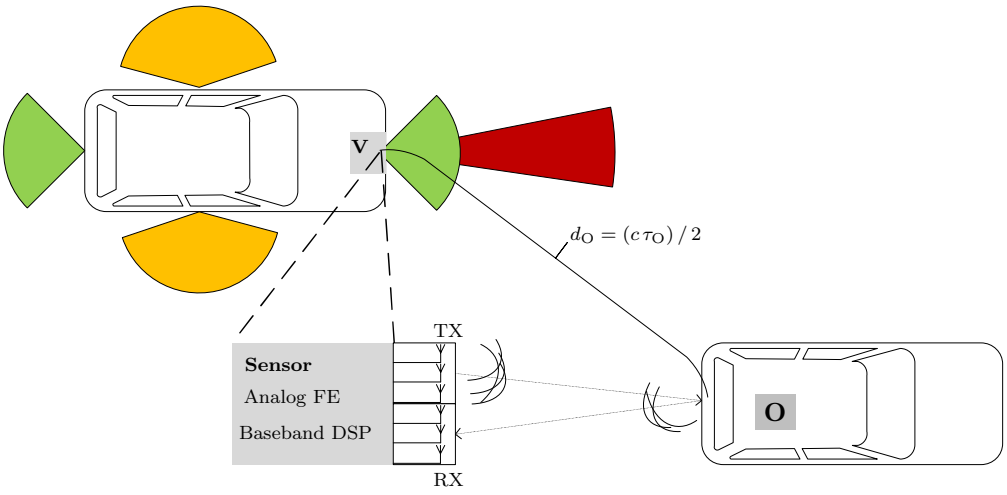

Figure 1.1: Depiction of the usage of radar in a modern vehicle and of the sensing principle. The sensor commonly incorporates the analog FE (Front End) and a DSP (Digital Signal Processor).

Additionally, an object and a "zoomed-in view" of a sensor with its working principle is visible. The sensor is denoted by **V**. It is detecting another vehicle, denoted by **O**. The sensor is of a *monostatic* configuration, meaning it incorporates transmission (TX) and reception (RX) at (approximately) the same spatial location. The principle is to transmit an electromagnetic wave, that is then reflected off of the object. This reflection is then received. By some measurement of the time delay between transmission and reception τ_O, the *object distance* (also termed *range*)

d_O can be assessed as

$$d_\mathrm{O} = \frac{c\,\tau_\mathrm{O}}{2}, \tag{1.1}$$

where c is the speed of light.

Eq. (1.1) measures the *radial distance*, as indicated in Fig. 1.1. To gather additional information about the exact location of an object, an *angle of arrival* measurement can be made when using several TX and/or RX channels [4]. Fig. 1.1 depicts the *antenna arrays* for the purpose of such a MIMO (Multiple Input Multiple Output) processing.

Also the *velocity* of objects provides key information for automotive radar applications. The relative radial velocity of an object can be extracted by measuring a frequency shift due to the Doppler effect, or possibly by comparing a number of consecutive measurements. [4].

The exact properties of the radar and the required processing of course depend on the used *waveform* and *signaling*. While alternative techniques have been proposed for modern automotive radar applications [5, 6], the CS (Chirp Sequence) variant of an FMCW (Frequency Modulated Continuous Wave) signaling scheme is the current de facto state of the art. This thesis therefore focuses solely on FMCW/CS radars.

1.1.1 Signal Processing in FMCW/CS Radar

Linear FMCW signals [7] are a popular choice for automotive applications due to their good range resolution and simultaneous range and Doppler measurement capabilities. Ambiguity as well as complexity issues arise when dealing with multi-object scenarios, however, for which several modifications to the signaling scheme were proposed [8]. In [9], a method is presented based on a rapid sequence of equivalent signals and subsequent two-dimensional FFT (Fast Fourier Transform) processing, which became known as CS radar.

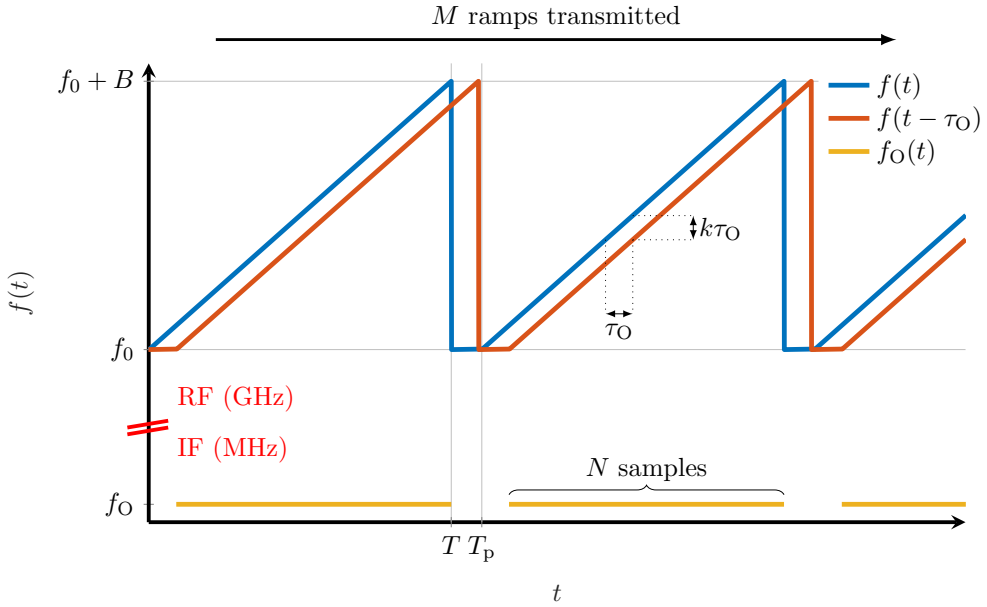

Figure 1.2: Illustration of the CS principle and object frequency course through the mixing process.

As Fig. 1.2 illustrates, the transmitted signal linearly frequency modulated as

$$f(t) = f_0 + kt\,,\; t \in [0, T]\,. \tag{1.2}$$

Parameters are the starting frequency f_0, slope k and duration T. The slope can also be defined

in terms of duration and bandwidth as $k = B/T$. We will refer to one such transmit signal as a *chirp* or a *ramp*. In CS radar, a sequence of M such chirps are transmitted. In real systems ramp transmissions do not begin immediately after each other, therefore we define a total "chirp repetition time" T_p as indicated in the figure.

The received signal is then for a single point object a delayed version of the ramp (sequence). A key observation is that this time delay corresponds to a constant *frequency offset*

$$f_\mathrm{O} = k\tau_\mathrm{O} \tag{1.3}$$

between the transmit and corresponding receive ramp. This frequency f_O is often termed *beat frequency*, but will also be called *object frequency* in this work. The object frequency can be "extracted" by a process of *mixing* TX and RX signal. After a band-limiting low-pass AAF (Anti-Aliasing Filter), the result is a signal of frequency f_O. The mixer's inputs are in the RF (Radio Frequency) domain, while its result after filtering is the so-called IF (Intermediate Frequency) signal. The bandwidth of the AAF is commonly referred to as the IF bandwidth B_IF. The IF signal is then sampled with a frequency $f_\mathrm{s} \geq 2B_\mathrm{IF}$. N samples per ramp are obtained for further digital processing. The obtained *object IF signal* at a single certain ramp with index m_i is therefore

$$s_\mathrm{O}^{(m_i)}[n] = A_\mathrm{O} \cos\left(2\pi \frac{f_\mathrm{O}}{f_\mathrm{s}} n + \varphi_0^{(m_i)}\right), \tag{1.4}$$

where A_O is the amplitude, and φ_0 a phase term.

Note that although actual further processing is clearly done on sampled signals such as (1.4), continuous descriptions (time t, frequency f) will be used throughout this thesis wherever it simplifies notation or explanation. Unless otherwise noted, the "discretization" of such results is straightforward.

To extract object distance information, we can then simply compute a DFT (Discrete Fourier Transform) of $s_\mathrm{O}^{(m_i)}[n]$. By detection and frequency estimation, a distance value can be computed as per (1.3) and (1.1).

Eq. (1.4) is strictly speaking only correct for static objects. An object moving with some velocity v_O causes the time-delay τ_O to change during transmission, introducing a Doppler frequency shift, as well as additional time-dependent phase terms into the equation. However, these terms can be essentially neglected with the condition of fast measurement compared to the movement of the object, as well as a high carrier frequency compared to the bandwidth. What remains is a phase term describing the *change between ramps*

$$\varphi_0^{(m_i)} - \varphi_0^{(m_i-1)} = \Delta\varphi_0 = 2\pi \frac{2 f_0 v}{c} T_\mathrm{p}, \tag{1.5}$$

indicating that an estimate of object velocity can be made by estimating $\Delta\varphi_0$.

If the IF signals of M ramps are then arranged in a matrix as seen in Fig. 1.3 , a DFT can be first computed for every column. This step is called *range compression*, obtaining the frequency spectrum corresponding to distance for each ramp. The samples of each respective ramp (column) are also referred to as *fast-time samples*.

At the row of the resulting matrix n_O corresponding to the object frequency f_O, the values are then

$$S_\mathrm{O}^{(m)}[n = n_\mathrm{O}] = A\mathrm{e}^{\mathrm{j}\Delta\varphi_0 m}. \tag{1.6}$$

Hence, (1.6) is a complex exponential with a (normalized to a sampling frequency of $1/T_\mathrm{p}$) frequency $\Delta\varphi_0$. By computing a second Fourier transform over the indices m, a peak at a *"Doppler frequency"* corresponding to a velocity via (1.5) is obtained. Note the assumption that n_O stays constant for every column of the range-compressed matrix. The samples over each

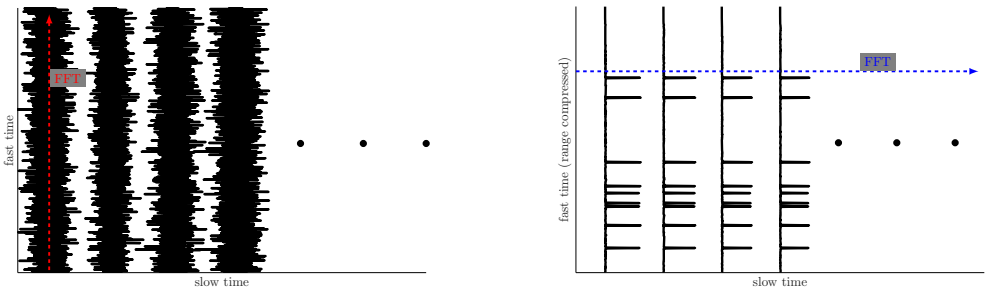

(a) Time-domain signals prior to RD (Range-Doppler) processing.

(b) Range-compressed matrix (after the first FFT, magnitude values).

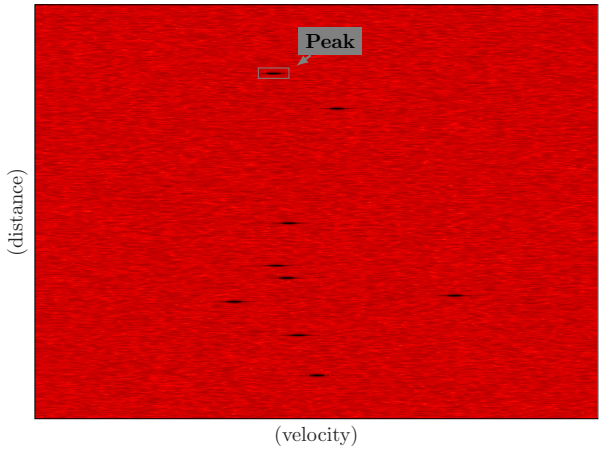

(c) Complete RD map (magnitude values). One of the peaks is highlighted.

Figure 1.3: Illustration of RD processing for an example with 9 objects. The arrangement into a matrix form and the directions of FFT processing are indicated accordingly.

respective row as input to the second FFT are also referred to as *slow-time samples*.

To summarize the basic steps of processing, the following is done:

- Measurement of M consecutive ramps of N samples, representing the time domain IF signal $s_{\mathrm{IF}}(t)$.
- Arrangement into a matrix form of size $(N \times M)$. As noted before, a continuous-time notation might still be used, as well as the notation $s_{\mathrm{IF}}^{(m)}[n]$.
- An optional time domain preprocessing step. Time domain interference mitigation methods to be introduced in Chapter 3 are a part of this step, yielding a processed signal $\tilde{s}_{\mathrm{IF}}(t)$. Other preprocessing steps include *windowing* and *zero-padding* (windowed signals will be denoted by $s_{\mathrm{win}[n]}$, zero-padded ones by $s_{\mathrm{zp}[n]}$).
- Usage of an FFT algorithm to transform each column of the matrix, obtaining *range* information through the frequency spectrum $S_{\mathrm{IF}}(f)$.
- Similarly, row-wise FFT of the matrix, obtaining *Doppler* information. The resulting matrix can be interpreted as a two-dimensional spectrum of distance and velocity, $S_{\mathrm{IF}}(d, v)$.
- Applying some peak detection technique on the Range-Doppler map, an identified point corresponds to a certain distance d_{O} and velocity v_{O}.
- The determined object values are used for further processing. Angle estimation yields the value of θ_{O}. Distance, velocity and angle may together be used for clustering, classification, and other tasks.

This is the core of signal processing in FMCW/CS radar, termed *Range-Doppler processing*. The matrix form of the spectrum is also called the *Range-Doppler map*.

Provided that the underlying assumptions as mentioned before are correct, the resolution sufficiently high and object reflections sufficiently strong, RD processing yields unambiguous distance and velocity values for a possibly large number of objects. Exact descriptions and derivations of the processes dealt with in this section can be found in [7, 9].

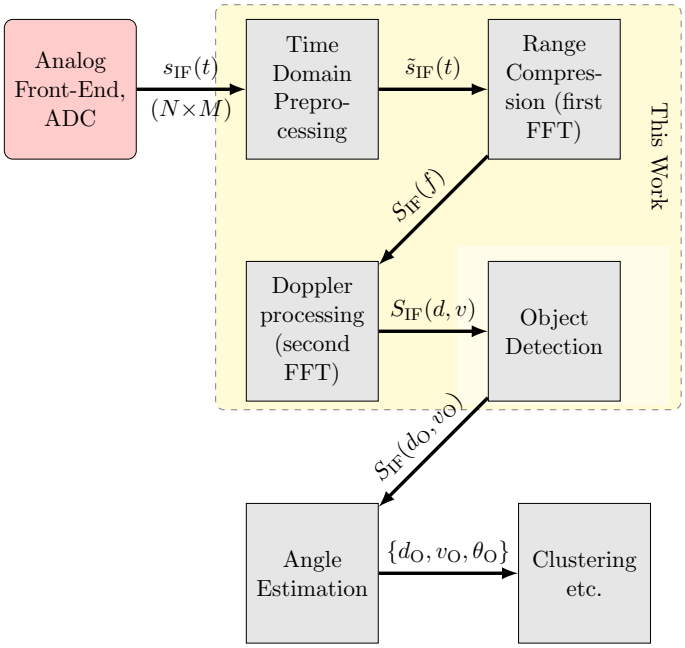

Figure 1.4: Basic CS radar signal processing chain. Elements that are the focus of this work are indicated accordingly.

Fig. 1.4 illustrates the complete low-level FMCW/CS signal processing chain. The analog part with a mixing and filtering step is indicated. Afterwards, *object peaks* are found by RD processing as explained before. In a MIMO configuration, the values of the object peaks at the different receive channels are processed for angle estimation. In addition, detected peaks can be clustered and classified as belonging to certain objects, to be used for higher-level tasks such as sensor fusion [10].

The scope of this work is also indicated in the diagram. Some investigation of analog aspects is done in the context of signal modeling. However, most of the focus will lie on RD processing. Higher-level functionalities, while certainly important, are only briefly mentioned.

1.1.2 The Issue of Interference

The previous section has discussed the signal processing principles in FMCW/CS radar. Naturally, the receive signal generated by an object was used to describe radar operation. However, any signal which lies inside the IF bandwidth at the ADC (Analog-to-Digital Converter) input during the time of measurement will be processed. Since the goal of the system is to identify objects, these other signals will act as a *disturbance*, generally decreasing detection performance. A simple classification of such disturbances can be the following.

- Noise – Thermal noise inherent at the antenna, the amplifier and every other electronic component.
- Clutter – The collection of a large number of non-essential signal reflections present in a practical radar application scenario (e.g. ground, raindrops, insects). These are neglected,

or rather considered as part of the receiver noise floor in this thesis.

- **Interference** – Any signal originating from other electronic devices sharing the same frequency band.

We model therefore in total the receive IF signal as

$$s_{\mathrm{IF}}^{(m)}(t) = \sum_{o=1}^{N_{\mathrm{O}}} s_{\mathrm{O},o}^{(m)}(t) + \sum_{i=1}^{N_{\mathrm{int}}} s_{\mathrm{int},i}^{(m)}(t) + n^{(m)}(t), \tag{1.7}$$

with N_{O} and N_{int} the number of objects and interferers, respectively, and $n(t)$ a receiver noise term.

This thesis focuses on interference, in particular on the *mutual interference* of radar sensors. For automotive radar, mutual interference is expected to become a very significant issue, due to the large number of sensing vehicles in the near future [3].

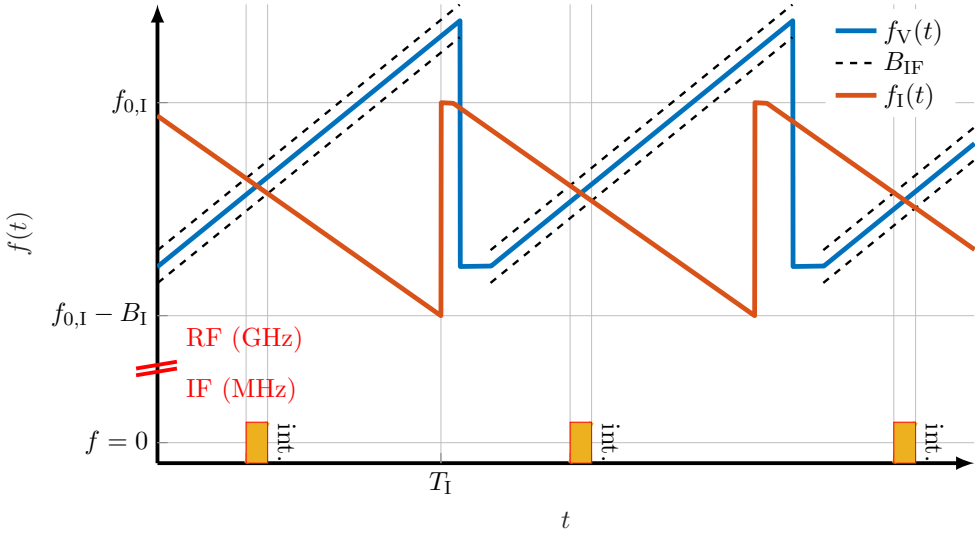

Figure 1.5: Illustration of the principle of non-coherent mutual CS radar interference.

The exact effect of interference of course depends on the form of the interfering signal. Fig. 1.5 indicates an example of mutual interference between two FMCW radars, which is the subject of this work. It can be said that during the time the transmit signal of the interfering radar is inside the receiver bandwidth, the measurement signal is distorted. The sensor suffering from the effect of the *interferer* is termed *victim*.

Depending on the *ramp parameters* (T, B, as introduced before) of victim and interferer, there are fundamentally two types of interference.

- If the occupied RF spectra and the slopes $k_{\{\mathrm{V,I}\}}$ are equal, the interfering ramp is parallel to the victim's transmit ramp. This means that it is essentially of the same form as an object reflection, as seen in Fig. 1.2, leading to so-called *coherent interference*. It possibly results in the detection of a *"ghost target"* on the RD map. Without some sort of prior knowledge, such a form of interference is completely indistinguishable from an object signal. This means that only higher-level mitigation methods, such as interference avoidance [11], are effective.

- In all other cases, as depicted in Fig. 1.5 , the ramps might "cross" at some point during the measurement. This is termed *non-coherent interference*, and leads to some *time-limited distortion* of the measurement signal, which will be referred to as a *burst*. For

such interference, it is possible to apply signal processing techniques before/during RD processing in order to mitigate its effects.

Since the focus of this work lies on low-level signal processing, non-coherent interference is the topic of this thesis. While coherent interference is certainly an important issue, not only are the possible mitigation approaches of a different type, it is also expected to be significantly less probable to occur than its non-coherent counterpart [12]. However, more investigation on such topics is needed, as well.

1.1.3 Research Questions and Objectives of this Thesis

We have introduced signal processing in CS radar and briefly illustrated its capabilities in Section 1.1.1. However, the detection of objects is only reliable for any system if the processed signal is sufficiently "clean", meaning free of the disturbances as introduced in Section 1.1.2. Automotive radar in the context of ADAS and autonomous driving is a highly safety-relevant component. If an object is not detected due to mutual interference, it might in fact lead to a *danger to human life*. Therefore, it is crucial to consider interference mitigation as an issue to be addressed in the design of future automotive radar sensors. Together with other measures to be taken, mitigation by signal processing methods is a reasonable approach.

This brings us to the main research questions addressed in this work.

- Can the effects of mutual interference on the performance of an automotive radar sensor be described from an in-depth signal processing point of view?
- Based on said description, can general statements be made about the effectiveness of different interference mitigation methods? Can a (from a certain perspective) "best" algorithm be found as a result of such a comparative analysis?

As a part of providing answers to the questions above, a key point of this thesis includes an analysis of mitigation methods. The goal is to treat state of the art methods in a comprehensive manner, yielding novel insights. A minor discussion of novel algorithms and improvements to existing techniques is also included throughout the work.

1.2 Related Work

One of the earliest treatises on the topic of mutual automotive radar interference can be found in [13]. Through interference scenario modeling and simulation, the authors come to the conclusion that mutual interference will be a significant issue to be considered when the percentage of radar-equipped vehicles becomes large. Another early discussion is given in [14], wherein some signal processing mitigation methods (zeroing, interpolation) are mentioned, as well.

In terms of interference modeling, [12] provides an early overview of the issue for FMCW (as well as pulsed) radar. An expression for the received interference power is given. In particular for FMCW, coherent and non-coherent interference of ramps as described in Section 1.1 is introduced and an estimate for their probabilities of occurrence is given. Similar discussions are found in [15,16]. In [17], an extension of such an analysis is done for the CS (RD processing) case. Analytical expressions for the interference power, object power and the processing gain lead to an estimation of the operating range of interfered FMCW radars in [18]. Mathematical formulations of non-coherent interference can be found in [19–21], as well as in several papers presenting mitigation methods, to be cited below. Investigations concerning coherent interference are also ongoing, with a recent contribution for the evaluation of ghost target probability [22].

A statistical description of traffic scenarios with respect to interference probability and power is presented in [23]. Most approaches, however, use a numerical simulation environment to

generate the traffic scenario with ray propagation models to investigate interference [24–27]. A hardware tool to generate interference for standardized sensor testing purposes is introduced in [28]. Another important development to note was the EU-project MOSARIM [29]. The project encompassed a definition of a list of interference traffic scenarios [30,31], a measurement campaign, simulation models [32] as well as a study on mitigation techniques [33].

Concerning active interference mitigation using signal processing algorithms, zeroing the affected samples can be considered one of the simplest methods. It, therefore, has been discussed in several publications [14, 20], often to compare its performance with a more advanced technique. Inverse windowing, a variant of zeroing, was discussed together with methods for the detection of interfered samples in [34, 35]. Other published proposed methods include variants of time domain subtraction [36,37], IMAT (Iterative Method with Adaptive Thresholding) [38], and Ramp Filtering [39]. The above methods will be discussed in this work, along with some others, in Chapter 3. Additionally, for a MIMO processing framework, interference mitigation by digital beamforming techniques has been presented [40, 41]. In terms of interference avoidance, techniques relying on a ramp-wise change of transmit signal parameters [42,43], as well as frequency hopping [11] have been discussed.

1.3 Outline of this Thesis

This work is structured in five main chapters as well as an appendix. **Chapter 1** contains this introduction. **Chapter 2** presents an in-depth analytical signal model of non-coherent interference, verified by simulation as well as measurement. Sections 2.1 to 2.3 discuss the interference signal at subsequent points of the RD processing chain, respectively. Section 2.4 compares the model to measured signals. Section 2.5 is a brief investigation of the received interference power and an outlook on its effects in a traffic scenario is given in Section 2.6.

Chapter 3 provides a summary and discussion of State of The Art mitigation methods. Section 3.1 classifies and groups algorithms according to meaningful aspects and Sections 3.2 to 3.6 investigate each technique separately.

Chapter 4 gives a comparative analysis of mitigation processing. It is mainly based on Monte Carlo simulations, enabling a statistical analysis of algorithm performance. Insights from the previous chapters are used to define a number of performance measures in Section 4.1, which are then evaluated in Section 4.2. The chapter also includes a brief discussion of the application of mitigation methods to measurements in Section 4.3.

Chapter 5 summarizes the results of this work and discusses aspects that may be the goals of future research. Last, **Appendix A** contains a brief description of the measurements conducted as part of the thesis.

2 Interference Modeling

In Chapter 1, we have introduced the signal processing chain for automotive radar and briefly discussed how interference affects the received signals. In the sequel, a more exact signal-level description of interference will be given. Section 2.1 introduces the model for the time domain *interference IF signal*. The sections that follow describe its form at the different stages of RD processing. In Section 2.2, the frequency spectrum of a single interference burst is derived, while Section 2.3 discusses the RD map of an interferer ramp sequence. Section 2.4 compares these theoretical results with measurement data. Section 2.5 discusses the aspect of received interference power in actual radar scenarios, and Section 2.6 illustrates a simulated example of such a scenario.

This chapter is strongly based on [44]. Similar results to the ones presented in Sections 2.1 and 2.2 can be found in [19]. The described model is, however, the result of independent research conducted by the author prior to awareness about the now cited work.

2.1 Effects in Time Domain

2.1.1 RF Signal Model

We consider the interaction of the victim sensor and an interfering radar. Both of them transmit an FMCW signal with a linear frequency course of $f(t) = f_0 + kt$ for some interval $t \in [t_{\text{start}}, t_{\text{end}}]$, with f_0 the starting frequency and k the slope. Fig. 2.1a illustrates an example of such frequency courses. Without loss of generality, only positive slopes are considered in the following.

The basic time domain signals in the RF domain are given as

$$s_{\{\text{V,I}\}}(t) = A_{\{\text{V,I}\}} \cos\left(2\pi f_{0,\{\text{V,I}\}} t + \pi k_{\{\text{V,I}\}} t^2 + \varphi_{0,\{\text{V,I}\}}\right), \tag{2.1}$$

where the subscripts V, I denote victim and interferer, respectively, and φ_0 is the arbitrary starting phase of the transmit signal. A signal of the form given in (2.1) is referred to as a chirp.

The ideal receiver multiplies the signal $s_{\text{V}}(t)$ with the received signal and filters the result limiting it to the frequencies $f \in [-B_{\text{IF}}, B_{\text{IF}}]$, where B_{IF} is the IF bandwidth. A derivation of the mixing process can be found in the previously mentioned references [15, 39].

The received signal is a superposition of object reflections and possibly several different interference signals. Since we are only interested in the general effect of interference on the IF signal, we consider only $s_{\text{I}}(t)$ at the mixer input and henceforth refer to the result of its mixing as the interference IF signal. For this, the arguments of the cosines in (2.1) are essentially subtracted at the points where the frequency of $s_{\text{I}}(t)$ is inside the IF bandwidth.

2.1.2 IF Signal Model

It can be seen from Fig. 2.1a that the frequency course of the interference IF signal, which will be termed $f_{\text{int}}(t)$, traverses the range $[-B_{\text{IF}}, B_{\text{IF}}]$. This is generally true except for the rare case

where the interfering ramp starts or ends inside the IF bandwidth, which will be neglected first. We define the time the ramp takes to traverse the range $[0, B_{\mathrm{IF}}]$ as T_{int}. The duration of the interference burst is then $2T_{\mathrm{int}}$; its slope is given by $k_{\mathrm{int}} = B_{\mathrm{IF}}/T_{\mathrm{int}}$.

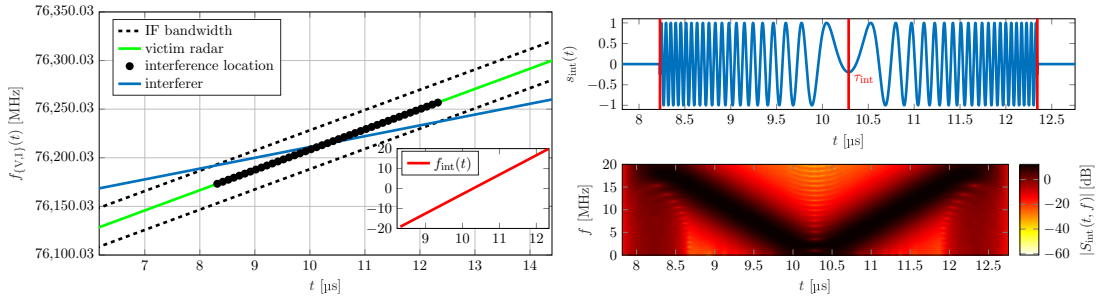

(a) Frequency courses and interference *(b) Interference IF signal and its spectrogram*

Figure 2.1: The parameters used in the simulation were the following: $f_{0,\mathrm{V}} = 76\mathrm{GHz}$, $f_{0,\mathrm{I}} = 76.1\mathrm{GHz}$, $k_{\mathrm{V}} = 20.833\mathrm{MHz}/\mu s$, $k_{\mathrm{I}} = 11.111\mathrm{MHz}/\mu s$ and $B_{\mathrm{IF}} = 20\mathrm{MHz}$, with the interferer and victim ramps starting at the exact same time.

Now, let τ_{int} be the point in time relative to the start of the victim radar's transmit ramp where the interference burst occurs, defined exactly as $f_{\mathrm{int}}(\tau_{\mathrm{int}}) = 0$. With this, the complete frequency course can be expressed as $f_{\mathrm{int}}(t) = -k_{\mathrm{int}}\tau_{\mathrm{int}} + k_{\mathrm{int}}t$ for $t \in [\tau_{\mathrm{int}} - T_{\mathrm{int}}, \tau_{\mathrm{int}} + T_{\mathrm{int}}]$, and therefore the time-domain interference IF signal (assuming unit amplitude) yields

$$s_{\mathrm{int}}(t) = \cos\left(-2\pi k_{\mathrm{int}}\tau_{\mathrm{int}}t + \pi k_{\mathrm{int}}t^2 + \varphi_{0,\mathrm{int}}\right). \tag{2.2}$$

An exemplary time domain interference IF signal is depicted in Fig. 2.1b. Eq. (2.2) is a simple model for the interference burst depending on parameters which may be estimated from the received IF signal. These parameters are connected to some of the actual transmit parameters of victim and interfering radar. The term $\varphi_{0,\mathrm{int}}$ encompasses a phase offset depending on the starting phases of the transmit and interfering chirps as $\varphi_{0,\mathrm{int}} = \varphi_{0,\mathrm{V}} - \varphi_{0,\mathrm{I}}$. Further, the slope of the IF signal is $k_{\mathrm{int}} = |k_{\mathrm{V}} - k_{\mathrm{I}}|$ as a result of the mixing process [20]. τ_{int} is determined partly by the relative starting times of transmit and interfering ramps which are arbitrary in real scenarios. For the special case of ramps starting at the exact same time, the relation $\tau_{\mathrm{int}} = (f_{0,\mathrm{V}} - f_{0,\mathrm{I}})/(k_{0,\mathrm{I}} - k_{0,\mathrm{V}})$ holds.

Note that in the spectrogram in Fig. 2.1b, because of the real cosine carrier, negative frequencies are mirrored onto their positive counterparts. This is assuming a real-valued receiver, which is common in automotive radar. Since the frequency course is an oddly symmetric function around the frequency zero, $s_{\mathrm{int}}(t)$ is actually an evenly symmetric signal around τ_{int}. This property will prove to be crucial for the analysis of its spectrum in the following section.

2.1.3 Extension to Other Cases

I/Q Demodulated Signal

With an I/Q-receiver, naturally $s_{\mathrm{int}}(t)$ is a complex signal, the real part of which was shown to be (2.2). It trivially follows that the imaginary part is a sin() function with the same argument as that of (2.2). Note that, in contrast to the real case, negative frequencies can be represented and hence do not get "mirrored". This means that linear frequency modulation from $-B_{\mathrm{IF}}$ to B_{IF} could be observed on a spectrogram such as the one depicted in Fig. 2.1b. This fact has a profound impact on the spectral characteristics of the interference signal, to be discussed in the next section.

Non-symmetric Signal

To generalize to cases where the interfering ramp does not traverse the complete range of $[-B_{\mathrm{IF}}, B_{\mathrm{IF}}]$, the expression of the frequency course and hence the reasoning leading up to (2.2) do not need to be changed. Even if no actual interference occurs at that point in time, τ_{int} can be uniquely defined, although its simple interpretation is lost. Eq. (2.2) is then valid in some interference interval $t \in [t_{\mathrm{start}}, t_{\mathrm{end}}]$, where $\tau_{\mathrm{int}} - T_{\mathrm{int}} \leq t_{\mathrm{start}} < t_{\mathrm{end}} \leq \tau_{\mathrm{int}} + T_{\mathrm{int}}$.

2.2 Effects on Range Spectra

At the range compression step of CS radar signal processing, the frequency spectrum of a ramp is computed. Therefore, to investigate the effect of interference on the resulting *range spectra*, we are interested in the spectrum of the interference IF signal $s_{\mathrm{int}}(t)$.

The computation of the Fourier transform can be facilitated by considering the following. Let

$$s_{\mathrm{int}}(t) = \begin{cases} s_{\mathrm{up}}(t) \text{ for } \tau_{\mathrm{int}} \leq t \leq \tau_{\mathrm{int}} + T_{\mathrm{int}} \\ s_{\mathrm{do}}(t) \text{ for } \tau_{\mathrm{int}} - T_{\mathrm{int}} \leq t < \tau_{\mathrm{int}}, \end{cases} \tag{2.3}$$

i.e., the signal $s_{\mathrm{int}}(t)$ is split into an up- and down-chirp. In the sequel, we consider the up-chirp first to derive the partial spectrum $S_{\mathrm{up}}(f)$, and then derive the spectrum of the whole interference IF signal (2.2) using the symmetry property noted in Section 2.1.2.

2.2.1 Spectrum of the Linear Up-Chirp

The up-chirp $s_{\mathrm{up}}(t)$ is a time-limited real-valued linear chirp. The Fourier transform of a signal of this sort can be evaluated analytically and yields a closed-form solution. It has been investigated for traditional pulse radar applications in [45].

In order to compute the Fourier transform $S_{\mathrm{up}}(f)$, the cosine is expressed in its complex exponential form. The integral can then be evaluated separately for the positive and negative exponentials. For the positive one we have

$$S^{+}_{\mathrm{up}}(f) = \frac{1}{2} \int_{\tau_{\mathrm{int}}}^{\tau_{\mathrm{int}}+T_{\mathrm{int}}} \mathrm{e}^{\mathrm{j}(-2\pi k_{\mathrm{int}} \tau_{\mathrm{int}} t + \pi k_{\mathrm{int}} t^2 + \varphi_{0,\mathrm{int}})} \mathrm{e}^{-\mathrm{j}2\pi f t} dt. \tag{2.4}$$

There are several ways to express the solution of (2.4). We choose to use the error function defined as

$$\mathrm{erf}(z) = \int_0^z \frac{2}{\sqrt{\pi}} \mathrm{e}^{-x^2} dx. \tag{2.5}$$

It is equivalently possible to use Fresnel integrals [46].

In any case, with the error function the spectrum can be expressed as

$$\begin{aligned} S^{+}_{\mathrm{up}}(f) = & \left(\frac{1}{4\sqrt{k_{\mathrm{int}}}} \right) \mathrm{e}^{\mathrm{j}\varphi_{0,\mathrm{int}}} \mathrm{e}^{\mathrm{j} \frac{-(2\pi k_{\mathrm{int}} \tau_{\mathrm{int}} + 2\pi f)^2}{4\pi k_{\mathrm{int}}}} \frac{1}{\sqrt{-\mathrm{j}}} \\ & \left[\mathrm{erf}\left(\sqrt{-\mathrm{j}\pi k_{\mathrm{int}}} \left(\tau_{\mathrm{int}} + T_{\mathrm{int}} - \frac{(2\pi k_{\mathrm{int}} \tau_{\mathrm{int}} + 2\pi f)}{2\pi k_{\mathrm{int}}} \right) \right) \right. \\ & \left. - \mathrm{erf}\left(\sqrt{-\mathrm{j}\pi k_{\mathrm{int}}} \left(\tau_{\mathrm{int}} - \frac{(2\pi k_{\mathrm{int}} \tau_{\mathrm{int}} + 2\pi f)}{2\pi k_{\mathrm{int}}} \right) \right) \right]. \end{aligned} \tag{2.6}$$

Naturally, the negative exponential yields a similar term $S^{-}_{\mathrm{up}}(f)$, with $S_{\mathrm{up}}(f) = S^{+}_{\mathrm{up}}(f) +$

$S_{\mathrm{up}}^{-}(f)$. Note, however, that the negative complex exponential determines the spectrum at the negative frequencies. Under the assumption that its "leakage" into the positive frequency axis is very small, we can neglect it and approximate $S_{\mathrm{up}}(f)$ by (2.6) for $f > 0$. This approximation is justified in [45] by the high center frequency of the chirp, which is not strictly given in the case of the IF signal in this work. Yet it proves to still be useful for our analysis in the following.

2.2.2 Spectrum of the Overall Interference IF Signal

We can use the symmetry properties of the Fourier transform to derive the spectrum of $s_{\mathrm{int}}(t)$ from (2.6). Since $s_{\mathrm{do}}(t) = s_{\mathrm{up}}(-t - 2\tau_{\mathrm{int}})$, it must hold for the Fourier transforms that

$$S_{\mathrm{do}}(f) = S_{\mathrm{up}}(-f) \exp\{-\mathrm{j}2\pi f 2\tau_{\mathrm{int}}\}. \tag{2.7}$$

It is also known that $s_{\mathrm{up}}(t)$ and $s_{\mathrm{do}}(t)$ are real signals, meaning $S_{\{\mathrm{up,do}\}}(-f) = S_{\{\mathrm{do,up}\}}{}^{\star}(f)$, where the star denotes the complex conjugate operation. From this, one can derive that

$$S_{\mathrm{int}}(f) = 2\,|S_{\mathrm{up}}(f)| \cos(\phi_{\mathrm{up}}(f) + 2\pi f \tau_{\mathrm{int}})\, \mathrm{e}^{-\mathrm{j}2\pi f \tau_{\mathrm{int}}}, \tag{2.8}$$

where $\phi_{\mathrm{up}}(f)$ is the phase of the spectrum of the up-chirp (alternatively, (2.8) is the real part of the spectrum of the up-chirp shifted to the origin). Hence we can deduce the following:

- The phase of the spectrum of the interference burst is linear, depending on τ_{int} only.
- The magnitude depends on the magnitude of the spectrum of the linear up-chirp component modulated by a cosine of its phase. This means that the magnitude changes in a highly dynamic manner. In the next section, said dynamic will be examined.

2.2.3 Magnitude Variation

The argument of the cosine term in (2.8) largely determines the variation in the magnitude of $S_{\mathrm{int}}(f)$. Thus, we invoke the approximation discussed in Section 2.2.1 and investigate the phase of the spectrum presented in (2.6). The terms constituting the phase of (2.6) can be separated into two parts. The arguments of the *complex exponential terms* $\phi_{\mathrm{exp}}(f)$, and the phase of the remaining terms, referred to as the *residual phase* $\phi_{\mathrm{res}}(f)$. Hence, we can write

$$\phi_{\mathrm{up}}(f) = \phi_{\mathrm{exp}}(f) + \phi_{\mathrm{res}}(f). \tag{2.9}$$

The residual phase is

$$\phi_{\mathrm{res}}(f) = \mathrm{atan2}\left(\frac{1}{\sqrt{-\mathrm{j}}} \frac{\Im\{\mathrm{erf}(C_1) - \mathrm{erf}(C_2)\}}{\Re\{\mathrm{erf}(C_1) - \mathrm{erf}(C_2)\}}\right), \tag{2.10}$$

where atan2() represents the four-quadrant inverse tangent and C_1, C_2 are the arguments of the error function terms as per (2.6). The term $1/\sqrt{-\mathrm{j}}$ yields the constant $\pi/4$. The error function term of (2.10) goes to zero as its argument goes to infinity [46]. For finite arguments, numerical simulations show that except for frequencies close to 0 and B_{IF}, the phase consists of relatively small fluctuations around zero [45]. Therefore we can assume $\phi_{\mathrm{res}} \approx \pi/4$.

The exponential terms (together with the term $+2\pi f \tau_{\mathrm{int}}$) can be simplified exactly to

$$\phi_{\mathrm{exp}}(f) = -\pi \frac{1}{k_{\mathrm{int}}} f^2 - \pi k_{\mathrm{int}} \tau_{\mathrm{int}}^2 + \varphi_{0,\mathrm{int}}. \tag{2.11}$$

Putting everything together and rearranging terms ultimately yields

$$|S_{\text{int}}(f)| \approx 2\,|S_{\text{up}}(f)|\,|\cos\left(\pi\frac{1}{k_{\text{int}}}f^2 + \pi k_{\text{int}}\tau_{\text{int}}^2 - \varphi_{0,\text{int}} - \frac{\pi}{4}\right)|. \tag{2.12}$$

Interestingly, the cosine term in (2.12) is a "chirp" in frequency with its slope being the inverse of the slope of the original chirp in time (in addition to some phase terms). Basically, for a fixed IF bandwidth B_{IF}, the longer the duration of an interference signal, the faster its resulting magnitude spectrum varies. The error due to our applied approximations can be generally said to be largest for small T_{int}, near the edges of the IF band. An example of the spectrum is shown in Fig. 2.2.

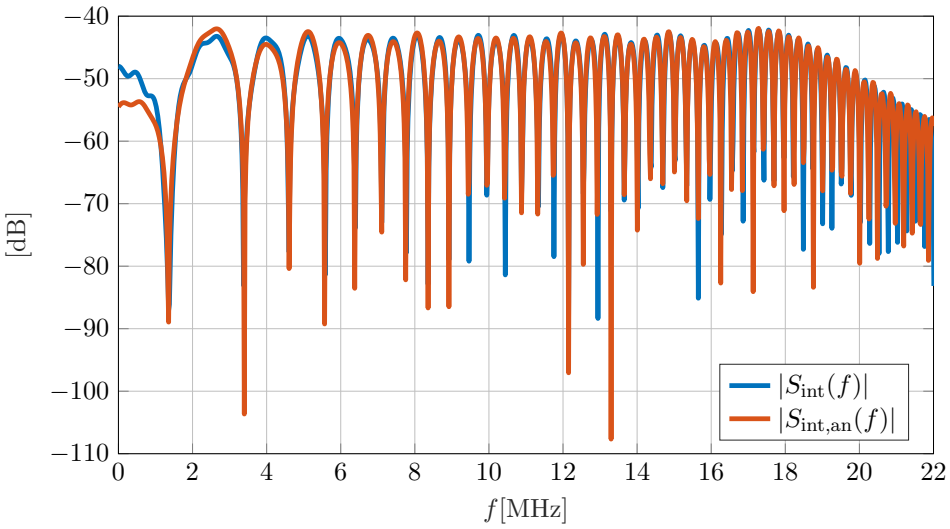

Figure 2.2: Magnitude spectrum from a system simulation $|S_{\text{int}}(f)|$ compared with the analytically derived approximation $|S_{\text{int,an}}(f)|$. Simulation parameters are the same as for Fig. 2.1.

2.2.4 Extension to Other Cases

I/Q Demodulated Signal

The case of a complex IF signal was briefly discussed in Section 2.1.3. For its spectrum, using the same decomposition $s_{\text{int}}(t) = s_{\text{up}}(t) + s_{\text{do}}(t)$ as previously, (2.6) is now an exact expression for $S_{\text{up}}(f)$, the spectrum of $s_{\text{up}}(t)$. Except for leakage due to the finite duration of the signal, said spectrum is limited to the positive frequencies. Considering that the time-domain symmetry still applies for the complex case, we can write

$$S_{int,IQ}(f) = S_{\text{up}}(f) + S_{\text{up}}(-f)\mathrm{e}^{-\mathrm{j}2\pi f 2\tau_{\text{int}}} \approx \begin{cases} S_{\text{up}}(|f|) \text{ for } f > 0 \\ S_{\text{up}}(|f|)\mathrm{e}^{-\mathrm{j}2\pi f 2\tau_{\text{int}}} \text{ for } f < 0 \\ 2S_{\text{up}}(0) \text{ for } f = 0. \end{cases} \tag{2.13}$$

As can be seen in Fig. 2.3, the approximation in (2.13) does not hold completely. Nevertheless, the symmetry in time translates to a symmetry of the magnitude spectrum $|S_{\text{int,IQ}}(f)| = |S_{\text{int,IQ}}(-f)|$.

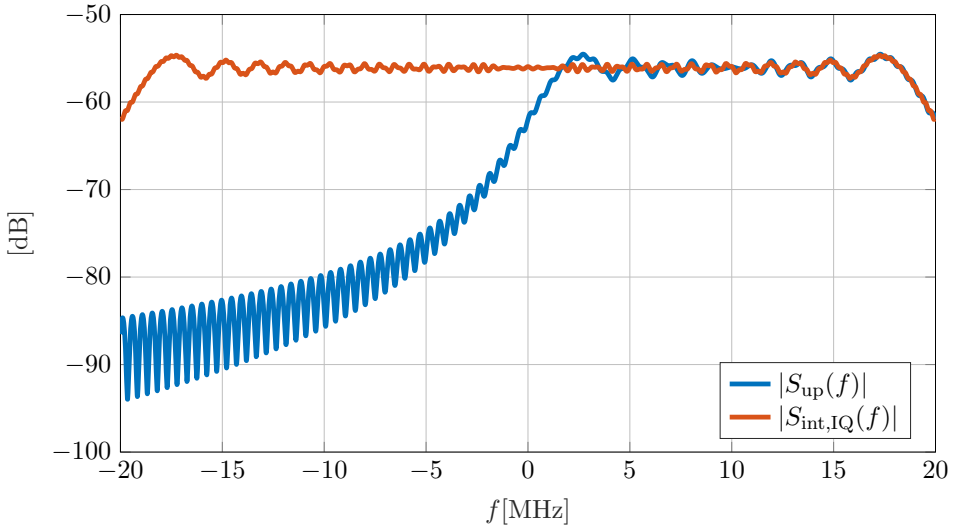

Figure 2.3: Depiction of the magnitude spectra of the "up-chirp" part $S_{\mathrm{up}}(f)$ and of the total symmetric complex interference signal $S_{\mathrm{int,IQ}}(f)$.

Non-symmetric Time-Domain Signal

As introduced in Section 2.1.3 as well, interference might not always result in a symmetric signal. This depends on when victim and interfering ramps "cross" (the reader may again refer to Fig. 2.1a). Since for this case no symmetry properties can be exploited in order to simplify or approximate the analytic expression for the spectrum, one can only evaluate the integral such as (2.4) inside the respective time limits.

Fig. 2.4 shows the up-chirp $s_{\mathrm{up}}(t)$ sliced into a number of pieces. A single slice of these could appear alone as a non-symmetric interference burst, having a certain center frequency and bandwidth. However, depending on the (generally short) duration, the signal is not strongly concentrated in frequency.

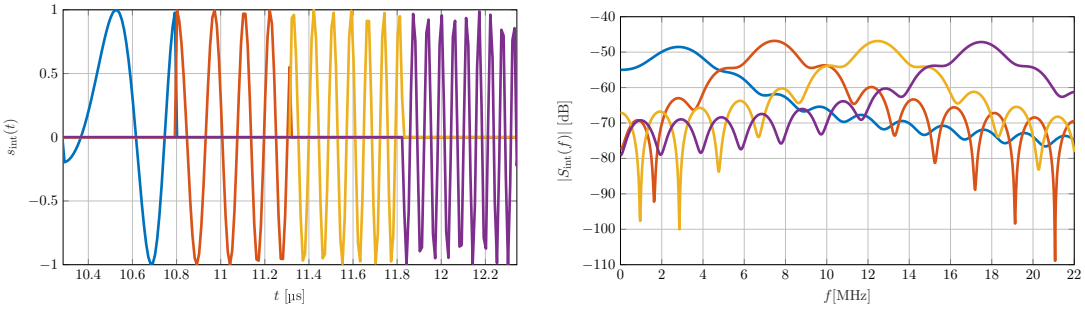

(a) Time domain signals *(b) Magnitude spectra*

Figure 2.4: An example of a linear up-chirp sliced into 4 parts of equal duration.

2.2.5 Practical Considerations

In the previous sections, a rather theoretical study was presented, based on an idealized continuous-time (and frequency) description. In the sequel, some aspects are briefly discussed that arise in a practical digital signal processing system. A discussion of other effects, e.g. that of amplifier non-linearity, can be found in [20].

Non-ideal IF Filter

In our model from Section 2.1, we implicitly assumed a perfect IF filter, completely band-limiting the signal to $[-B_{\mathrm{IF}}, B_{\mathrm{IF}}]$. This in turn defined the duration of the interference burst to be T_{int}. However, in practice the signal is filtered by a non-ideal analog AAF (the terms *IF filter* and *AAF* are used interchangeably in this work). Such a filter has an impulse response of infinite duration and a non-linear phase spectrum. The phase spectrum is assumed to be known and compensated for in the receiver.

The effects of filtering are briefly summarized below, as well as illustrated in Fig. 2.5.

- The amplitude of the time-domain interference IF signal, modeled in (2.2) as constant, decays depending on the filter type and order. This effectively increases the duration of the signal, which leads to a slight change in the spectrum due to the change of the value of T influencing (2.6).
- The envelope of the magnitude spectrum in (2.12) decays after the cut-off frequency of the filter with a rate depending on the filter transfer function.

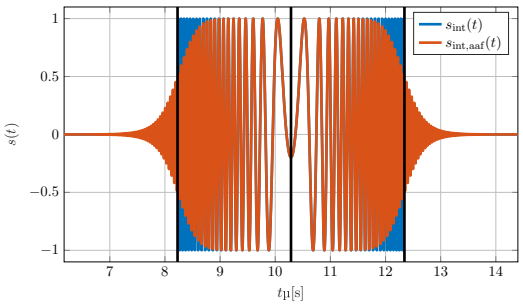

(a) Idealized interference signal $s_{\mathrm{int}}(t)$ and its (zero-phase) filtered version $s_{\mathrm{int,aaf}}(t)$.

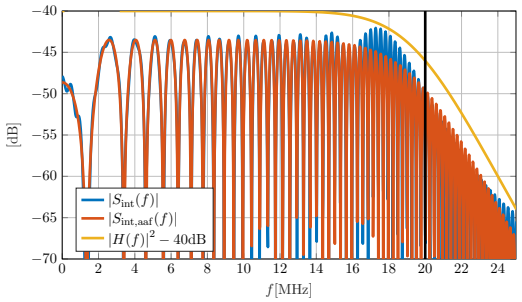

(b) Magnitude spectra corresponding to the time-domain signals, as well as the frequency course $|H(f)|$ of the filter itself.

Figure 2.5: Effect of the non-ideal IF filter.

Fourier Transform Representation

After analog filtering, the IF signal gets digitized and processed by computing a FFT of finite length N. We assume that no aliasing or other damaging effects (e.g., clipping) occur at or before the digitization stage. Before the transform, the signal might be windowed and/or zero-padded. There are two things to consider:

- The ability to resolve the zeroes of the modulation term in (2.12) is limited by numerical accuracy but gets better with an increasing number of samples. The difference between the original and zero-padded versions of the spectra can be seen in Fig. 2.6.
- Since the largest "chirp variation frequency" in (2.12) is T_{int} , to resolve the magnitude variation it has to hold that

$$\frac{N}{f_s} > 2T_{\mathrm{int}}, \tag{2.14}$$

where f_s is the sampling frequency of the receiver. Above expression however does not include a term for the case of windowing. The resolution decreases by some factor depending on the type of window. This is observed in Fig. 2.6 as an effect of averaging for higher frequencies.

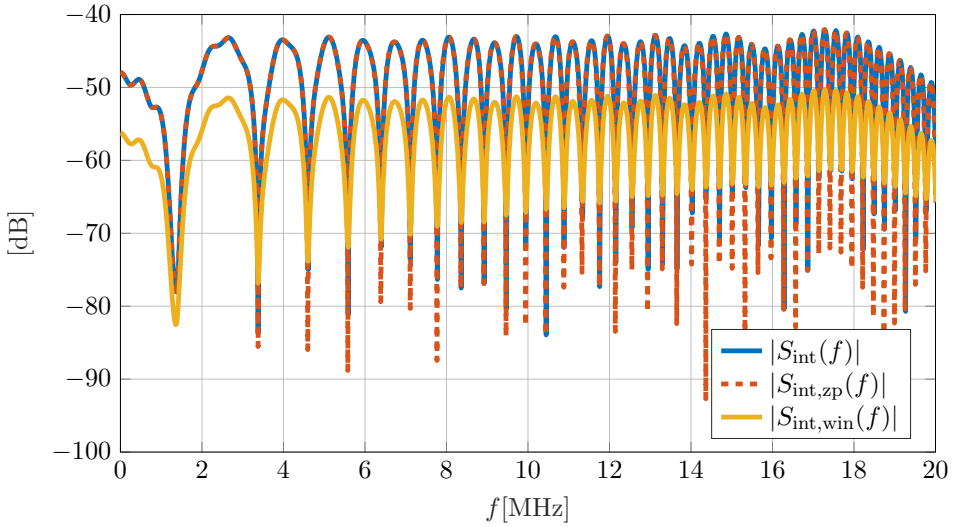

Figure 2.6: FFT magnitude spectra $|S_{\mathrm{int}}(f)|$ of the digitized signal $s_{\mathrm{int}}(t)$, a 10-fold zero-padded variant $s_{\mathrm{int,zp}}(t)$ as well as a Hann-windowed $s_{\mathrm{int,win}}(t)$. The FFT length is $N = 2400$. Other simulation parameters are the same as for Fig. 2.1.

Sensitivity to Parameters

As will be detailed in Section 3.4.1, an approach to cancel interference is to reconstruct the interference signal and subtract it from the total received IF signal as in [37]. Thereby ideally only useful signal components are kept. This is essentially an estimation problem of the parameters $\tau_{\mathrm{int}}, k_{\mathrm{int}}$ and $\varphi_{0,\mathrm{int}}$ in (2.2). A question we can pose is how accurately these parameters need to be estimated for a sufficient cancellation performance. Fig. 2.7 illustrates the effect of changing τ_{int} by a small amount. In fact, assuming a sampling frequency of $f_{\mathrm{s}} = 40\,\mathrm{MHz}$, the amount of change in τ_{int} relative to a sampling time interval is 2%. It can be seen that the signal form is very sensitive to these changes both in time and frequency domain. A simple expression for this local parameter change sensitivity is

$$\left| \frac{\partial s_{\mathrm{int}}(t = \tau_{\mathrm{int}})}{\partial \tau_{\mathrm{int}}} \right| \propto k_{\mathrm{int}} \tau_{\mathrm{int}}. \tag{2.15}$$

For our earlier chosen simulation parameters, (2.15) yields a factor of order 10^8, which is clearly a high sensitivity. Thus, parameter estimation might prove to be difficult using a relatively small number of noisy interference signal samples. Such issues are discussed in Chapter 3 more thoroughly.

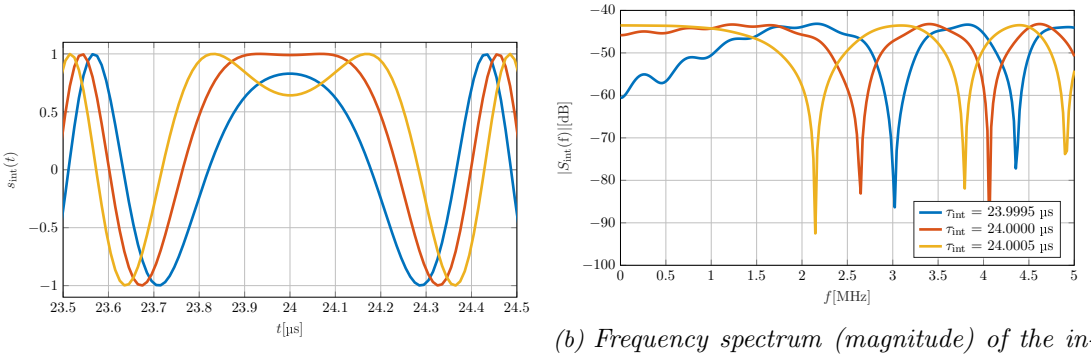

(a) Time domain interference IF signal

(b) Frequency spectrum (magnitude) of the interference IF signal

Figure 2.7: Simulation parameters were kept the same as for Fig. 2.1, except for τ_{int} being set to the values as can be seen on the legend.

2.3 Effects on the Range-Doppler Map

As we have seen in the previous section, interference has an effect of broadband distortion on the signal spectrum. It can be, at least for the most common case, described analytically by a relatively simple parametric model. However, as we have introduced in Chapter 1, in CS radar several ramps are arranged in a matrix before a subsequent FFT is computed across the ramps (slow-time domain). Since it is the RD map that is ultimately used for object detection, a view on interference on this level is needed.

Note that the time-domain input signal for every ramp is a simple sum of object and interferer signals, and all the operations that follow are linear. Hence, as in the previous sections, interference can be investigated independently. Fig. 2.8 is an illustration of the result of processing the signal coming from an interferer. From left to right, first we see the time-domain where some of the ramps are not interfered at all (hence a "zero signal"), while some of them contain a chirp burst as introduced in Section 2.1.2. In the middle, we see the corresponding range spectra, again of a known form. Lastly, the RD map is shown, the signal therein being of a much more noise-like, difficult to analytically describe, form.

The step yielding the RD map processes the signals defined across the ramps. A sample of such a signal is either zero (at the ramps where no interference took place) or some complex number according to the interference spectrum at that specific ramp and bin. While technically deterministic, the resulting interference RD map is dependent on the exact timing of victim and interference ramp patterns, and therefore a parametric model is hardly possible to derive. However, a statistical approach might lead to some general statements.

Considering the FFT operation, intuitively if there is a repeating pattern present in the values of the interference spectrum over the ramps, the FFT through its coherent integration will concentrate the energy at specific areas on the RD map. Conversely, the absence of any such pattern produces the noise-like map we can see in Fig. 2.8. Hence, another property of coherence can be defined, which we shall call *ramp-coherence* and briefly discuss further.

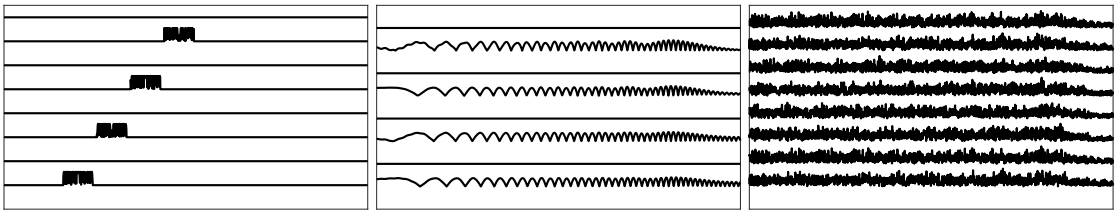

(a) Time-domain *(b) Range spectra* *(c) Range-Doppler map*

Figure 2.8: Example of an interference pattern (slice of 8 ramps out of the 128 actually processed). The magnitude of the signals in linear scaling is shown. Exact labeling is not included; this figure is only for the purpose of illustrating the principle.

2.3.1 Ramp-coherent Case

We define interference *ramp-coherent* if the pattern of interference bursts leads to a non-uniform distribution of interference energy on the RD map. It is difficult to make a quantitative statement about its occurrence. Essentially, a certain mathematical relationship between the ramp parameters of victim and interferer radar has to be present that leads to a strong correlation between the spectrum of interference at different ramp indices.

Intuitively, such a case might be thought to be rather rare in practice. It can be pointed out that the uncertainties inherent in the system (e.g., phase noise) lead to a significantly different interference spectrum at each ramp, due to the sensitivity described in Section 2.2.5. Nevertheless, more practical investigations would be needed to make accurate statements about this issue.

The effects of ramp-coherence will be shown based on an example constructed in simulation. Table 2.1 lists the relevant simulation parameters. Both ramp sequences start at the same point in time; as mentioned already, this is a rather extreme example. The start of the resulting repeating pattern can be observed on Fig. 2.9.

Parameter	**Victim**	**Interferer**
start frequency [GHz]	76	76.1
sweep bandwidth [GHz]	1	1
sweep time [µs]	48	90
idle time between sweeps [µs]	0	0
# ramps transmitted	128	128

Table 2.1: Parameters for the constructed example of ramp coherence.

Fig. 2.10a shows the result of range processing, from which we can already roughly visually infer the periodic appearance of similar spectra. This is then translated in Fig. 2.10b to a number of velocities where interference energy is more strongly concentrated.

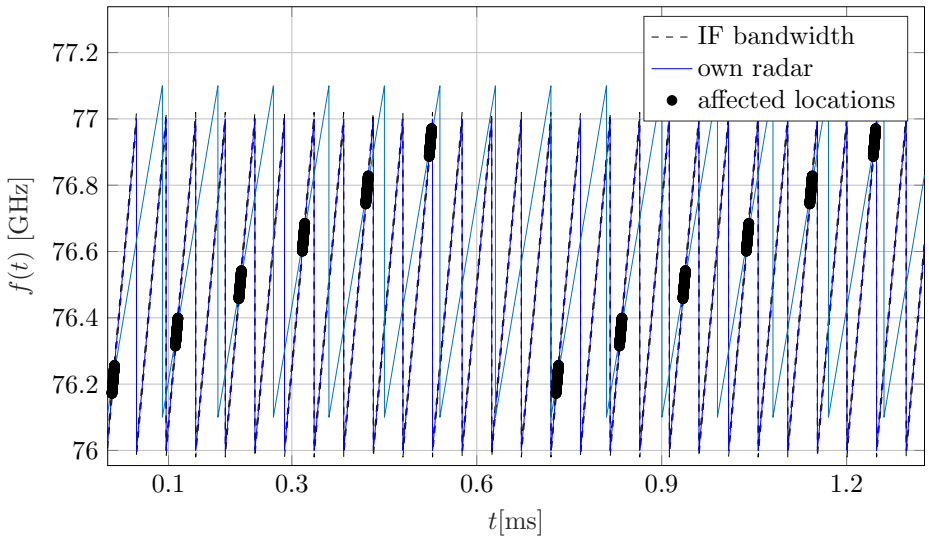

Figure 2.9: Slice of the resulting RF ramp pattern.

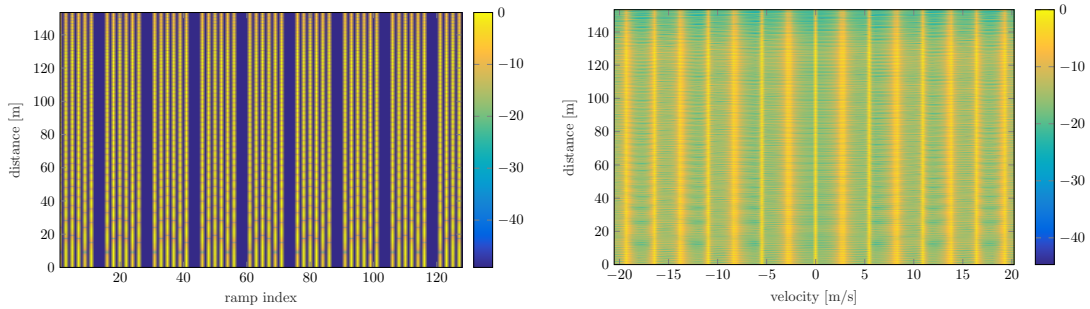

(a) Range spectra *(b) RD map*

Figure 2.10: Result of processing ramp-coherent interference. The colorbar shows a normalized [dB] magnitude value.

2.3.2 Ramp-incoherent Case

By changing the value of the sweep duration of the interferer from 90 to 90.3µs, the previously described ramp coherence strongly decreases, although this would constitute a very minor visual change in a depiction such as Fig. 2.9. This makes sense, since the arithmetic relationship between the values of ramp durations becomes more complicated.

The results can be seen in Fig. 2.11. On the range spectra, it is simplest to observe the zeroes of the different interfered ramps being less ordered when compared to Fig. 2.10a. This leads to a very noise-like RD map.

The lack of correlation between the ramps naturally leads to increased whiteness of the Doppler spectrum. In addition, the values seem to approximate a complex circular Gaussian distribution. A histogram of the real part and its least-squares fitted Gauss curve is illustrated on Fig. 2.12. The imaginary part behaves essentially the same way, and is not depicted here.

In general, it appears that an incoherent interference pattern of a large number of ramps/samples has a similar behavior to AWGN (Additive White Gaussian Noise). The more *ramp-coherence* is present, and the less samples are processed, the less the prior statement is true.

An explanation of this behavior is that the values of the spectra over the ramps at a certain range can be thought of as a "random sampling" of $S_{\text{int}}(f)$ from (2.8). The samples are approximately of uniform phase and of some non-trivial magnitude distribution. The FFT over a

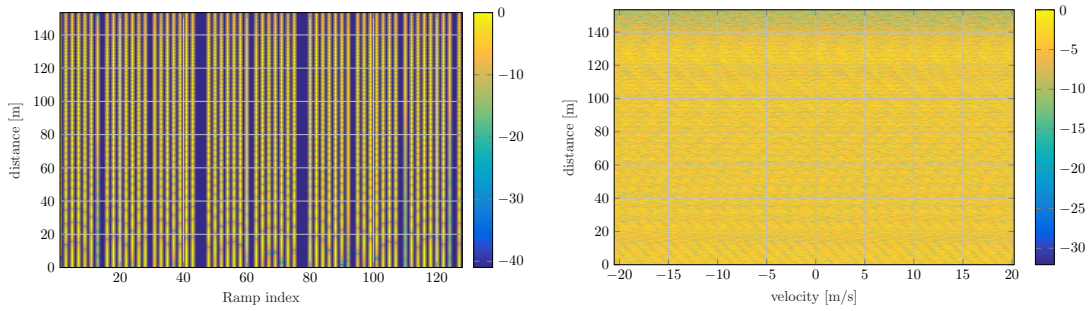

(a) Range spectra *(b) RD map*

Figure 2.11: Result of processing ramp-incoherent interference. The colorbar shows a normalized [dB] magnitude value.

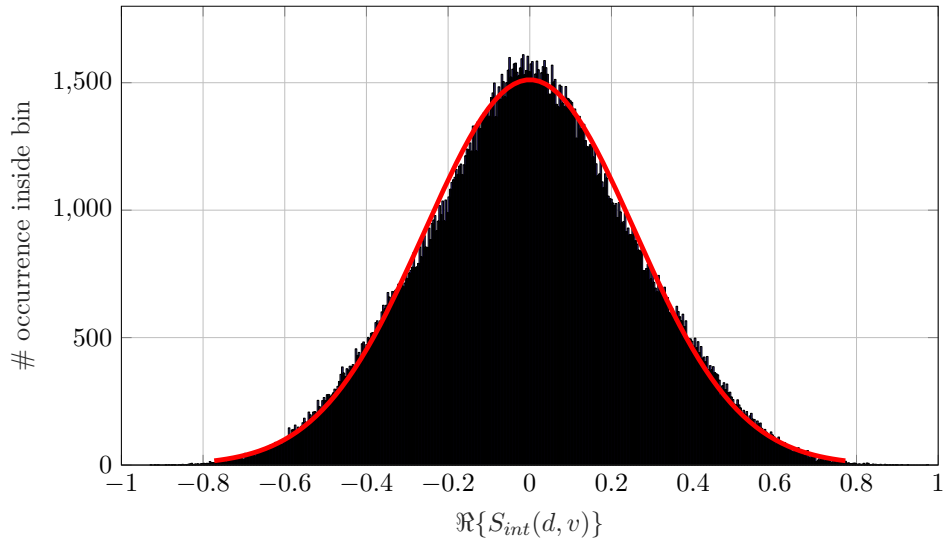

Figure 2.12: Histogram of the (normalized) real part of the values of the interference RD map, termed $S_{int}(d,v)$ here. In addition, a Gaussian fit is plotted (red). The size of the map was 2048×128.

sequence of such random samples then naturally, through an averaging effect, tends to a complex Gaussian distribution (essentially an embodiment of the Central Limit Theorem).

The statistical properties of both the real and imaginary parts of $S_{\text{int}}(d,v)$ can be approximated as

$$\hat{\mu}_{\text{RD}} \approx 0 \tag{2.16}$$

$$\hat{\sigma}^2_{\text{RD}} \approx P_{\text{int}}/2, \tag{2.17}$$

where P_{int} equals the total interference power over all ramps in the respective measurement, and μ_{RD} and σ^2_{RD} are mean and variance of the (hypothetical) AWGN on the RD map, respectively. Note that with the assumption of such an AWGN model, it becomes significantly simpler to make statements about detection probability in a certain scenario.

2.4 Experimental Verification of the Model

To conclude this chapter, the validity of the introduced signal model will be shown based on measurements. For a description of the exact measurement setup, please refer to Appendix A.1.

Due to the nature of the conducted measurement, no scenario-specific dynamics to be introduced in Section 2.6 will be discussed. The focus therefore is on the investigation of the effects derived in Sections 2.1 - 2.3.

2.4.1 Example of a Ramp Pattern

Let us first take a look at the processing of $M = 128$ consecutive ramps. The signaling parameters of victim and interferer are listed in Table 2.2. Note that the interferer actively transmits during both the up- and down-ramp (referred to as the "flyback phase"). This is not common in CS radar, and therefore has not been explicitly considered in this work before. In any case, it can easily be modeled as two sets of different ramp parameters, denoted by the subscripts I and I, down, respectively.

Variable	Set Value
$B_{\mathrm{IF,ENBW}}$	20MHz
f_0	76GHz
k	$k_{\mathrm{I}} = 7.813\mathrm{MHz/\mu s}$, $k_{\mathrm{I,down}} = 62.5\mathrm{MHz/\mu s}$, $k_{\mathrm{V}} = 6.25\mathrm{MHz/\mu s}$
T	$T_{\mathrm{I}} = 128\mu\mathrm{s}$, $T_{\mathrm{I,down}} = 16\mu\mathrm{s}$, $T_{\mathrm{V}} = 99.2\mu\mathrm{s}$
T_{p}	$T_{\mathrm{p,I}} = 205\mu\mathrm{s}$, $T_{\mathrm{p,V}} = 237\mu\mathrm{s}$
N	3968

Table 2.2: Measurement parameters for this example.

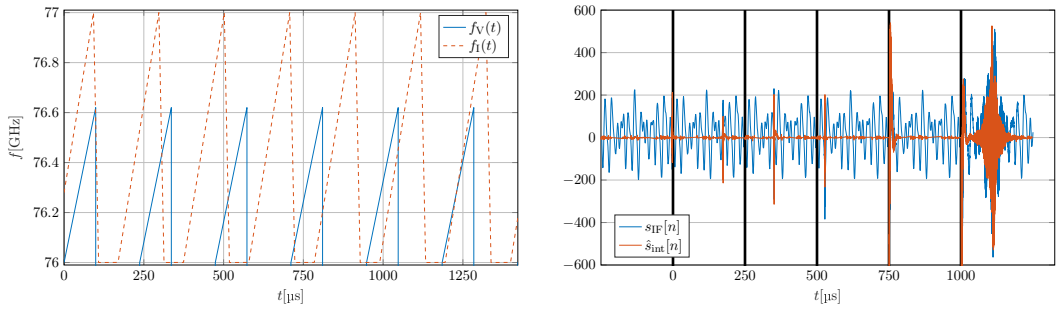

(a) Reconstructed frequency courses of victim and interferer (first 6 ramps).

(b) Received signals. Separate ramps are indicated by the thick vertical lines.

Figure 2.13: Reconstructed ramp pattern and the corresponding measured signals.

As expected, it can be seen in Fig. 2.13 that interference in fact appears according to the ramp pattern. Down-ramps lead to small bursts while interference of the two relatively similar up-ramps can be observed on the last section in the figure. Note that the initial delay between the ramp sequences was adjusted manually using the position of the first interference burst. In Fig. 2.13a, $s_{\mathrm{IF}}[n]$ is the original measured IF signal, while $\hat{s}_{\mathrm{int}}[n]$ is a recovered component containing interference (and noise) only. The recovery was done by subtraction of one of the interference-free signals, which leads to a reasonable result only since the scenario is completely static.

The interference components are then RD processed, the results being depicted in Fig. 2.14b. Both appear to match the previous considerations in Sections 2.2 and 2.3 generally very well. An expected difference from the idealized model is the effect of the analog high- and low-pass receiver filters, which are parts of the measurement hardware.

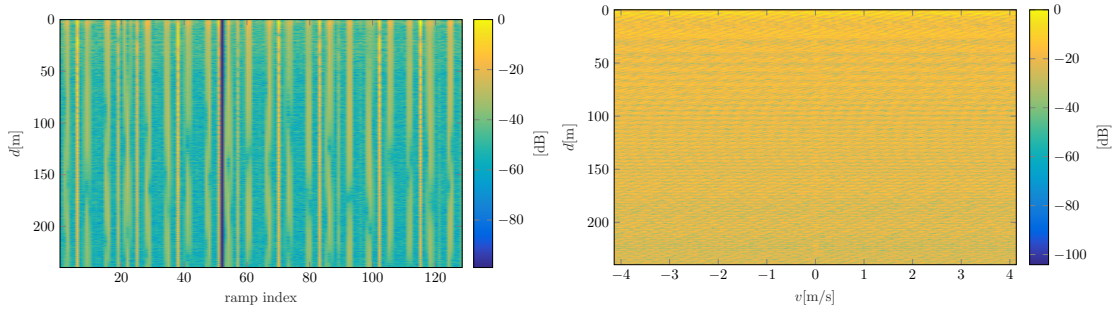

(a) Range spectra. *(b) RD map.*

Figure 2.14: Matrix (normalized magnitudes) after the first and second FFT stages, respectively. Ramp 52 has been subtracted from each received ramp before, including itself, hence the gap in (a).

2.4.2 Observation of a Measured Interference Signal

As an example of the exact signal form, a measured burst from an interfering up-ramp is taken. Here, the victim is set to a slope of $k_{\mathrm{V}} = 9.091\mathrm{MHz/\mu s}$. The signal then was filtered through a low-pass with a cut off frequency of 10MHz, as well as reverse-filtered through a high-pass. These steps were done in order to somewhat compensate for the effects of the analog filters.

The result is seen in Fig. 2.15 as $s_{\mathrm{int,meas}}(t)$. While there is still considerable asymmetry present due to the lack of accurate equalization, the characteristic "chirp-burst" form and its cosine-modulated magnitude spectrum are apparent on Figures 2.15a and 2.15c. As for the phase depicted in Fig. 2.15b, the form is strongly connected to the symmetry of the time-domain signal, and hence highly sensitive to its changes.

For comparison, a signal using the same victim and interferer ramp slope parameters was generated implementing (2.2), termed $s_{\mathrm{int,sim}}(t)$. The actual τ_{int} is unknown, so the burst was shifted in time to roughly align with the measured signal. The relative phase offset is naturally unknown as well, and was set simply to zero. Due to this misalignment, the precise features of both signals are very different, considering parameter sensitivity as already briefly discussed in Section 2.2.5. Nevertheless, a general similarity is observed. In particular, the duration T_{int} of the measured burst compares well to that of $s_{\mathrm{int,sim}}(t)$, being slightly larger caused by filtering.

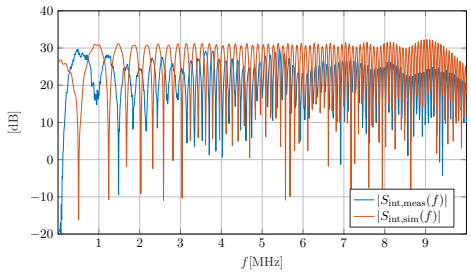

(a) Magnitude spectrum.

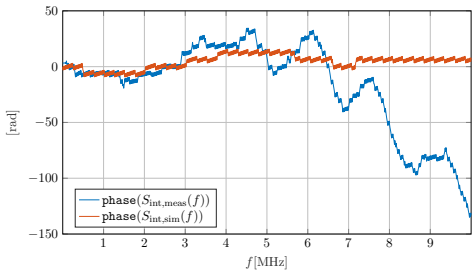

(b) Phase spectrum.

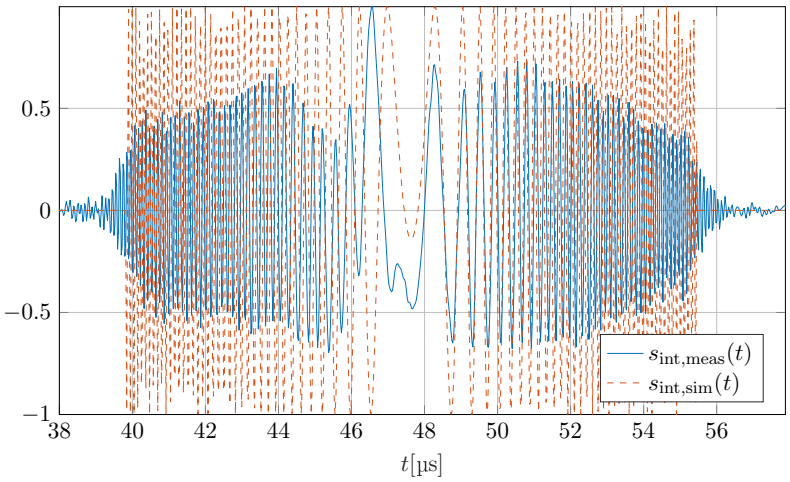

(c) Time-domain burst (zoomed-in view).

Figure 2.15: Example of a measured interference burst and comparison to ideal signal model.

2.5 Received Interference Power and Range-Doppler Processing Gain

A fundamental part of this thesis is the low-level description of interference signals, with which the previous sections of this chapter have been dealing. However, from a practical perspective, knowledge about the properties of interference occurring in actual (future) traffic scenarios is also essential. Particular interest is in the power of interference as received by the victim radar, compared to that of the objects, and subsequently its effect on detection.

Scenario analyses, and their incorporation into some statistical framework, is in general very difficult and out of the scope of this work. A limited body of work on experimental [26] and mathematical [18, 23] scenario modeling is found in the literature.

Nevertheless, a simple model has been implemented in our simulation framework. The received powers from an object $P_{\mathrm{RX,O}}$ and an interferer $P_{\mathrm{RX,int}}$, respectively, are defined as [12]

$$P_{\mathrm{RX,O}} = \frac{P_{\mathrm{TX,V}} G_{\mathrm{TX,V}} G_{\mathrm{RX,V}} \sigma_{\mathrm{O}} \lambda_{\mathrm{c}}^2}{(4\pi)^3 \, d_{\mathrm{O}}^4} \tag{2.18}$$

$$P_{\mathrm{RX,int}} = \frac{P_{\mathrm{TX,I}} G_{\mathrm{TX,I}} G_{\mathrm{RX,V}} \lambda_{\mathrm{c}}^2}{(4\pi)^2 \, d_{\mathrm{I}}^2}. \tag{2.19}$$

This model is derived from the classical quasi-monostatic radar equation, and has been explained and used in a similar way e.g. in [18]. As a value for the receiver noise floor, we use

$$P_{\mathrm{N}} = \kappa \vartheta B_{\mathrm{IF,ENBW}} F_{\mathrm{N}}, \tag{2.20}$$

which incorporates the well-known formula for thermal noise and a noise factor that accounts

for the receive path hardware.

The variables used in (2.18)- (2.20) are summarized in Table 2.3.

Variable	Description
P	power
G	gain (antenna)
σ	RCS (Radar Cross Section)
λ_c	carrier wavelength
d	distance
κ	Boltzmann constant
ϑ	antenna or ambient temperature
$B_\mathrm{IF,ENBW}$	ENBW (Equivalent Noise Bandwidth) of the receiver IF filter
F_N	NF (Noise Factor) of receive path

Table 2.3: Parameters for the interference scenario model. Unless otherwise specified, the subscripts TX *and* RX *stand for transmit and receive, respectively.*

Eq. (2.18) describes the power at the receive antenna feedpoint. In the receive chain, the signal is generally first amplified. This need not be explicitly considered for objects and interference (however, it is included in (2.20)), since we are ultimately only interested in the SINR (Signal-to-Interference-and-Noise Ratio), which is a relative value. Afterwards, by digitization, $N \times M$ samples are obtained. For simplicity's sake, let us assume that the average " sample energy", whether object signal or interference, equals the received power

$$P_\mathrm{RX} = \frac{\sum_\mathrm{N} |s[n]|^2}{N}. \tag{2.21}$$

Note that interference causes short bursts in the IF signal, while an object signal is present in all received samples. By RD processing, ideally the energy of an object signal is concentrated into a single sample on the resulting RD map (*not* taking leakage into account). On the contrary, interference energy becomes distributed more or less equally on the RD map, depending on the degree of ramp coherence. Therefore, the SINR on the RD map, corresponding to detection performance, is in general considerably higher than that at the receiver input. This can be modeled as a processing gain factor G_P

$$\mathrm{SIR} = \frac{P_\mathrm{RX,O}}{P_\mathrm{RX,int}} G_\mathrm{P}. \tag{2.22}$$

The value of G_P is then (with the assumptions and simplifications as mentioned before)

$$G_\mathrm{P} = \frac{(N_\mathrm{RD}/2)}{\left(\frac{N_\mathrm{RD,Int}}{N_\mathrm{RD}}\right)}. \tag{2.23}$$

The numerator in (2.23) is the gain due to the coherence of the object, $N_\mathrm{RD} = NM$ being the total sample size of the RD map. The denominator naturally is the "processing loss" of interference. The factor 1/2 in the numerator only applies with non-IQ processing.

2.6 Example of a Simulated Scenario

As part of the MOSARIM project [29], a number of traffic scenarios are presented, deemed by the authors thereof to be critical for interference. In the sequel, one of these scenarios is simulated and briefly analyzed to illustrate the effects discussed before.

Fig. 2.16 shows the chosen scenario. It is a rather simple one where the potential danger of interference can be easily recognized. The interferer (2) is relatively close right across the car carrying the victim radar (1), while a small RCS motorcycle (3) is in a slightly more distant position.

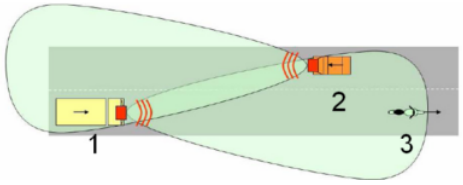

Figure 2.16: Scenario depiction, taken from [32] .

Table 2.4 summarizes the parameters used in this case. For simplicity, the interferer is not considered an object. We are only interested in the detection/estimation of the radial distance and velocity of the motorcycle and the effect of interference on it. The ramp parameters of the interferer are chosen randomly, and lead to ramp-incoherent interference. Do note that at every step, the simulation is reset such that the interference ramp pattern is the same; only the signal powers change.

Table 2.4: Simulation parameters for this example.

Variable	**Set Value**
d	$d_\mathrm{I} = 20.1\mathrm{m}, d_\mathrm{O} = 40\mathrm{m}$ (initial)
v	$v_\mathrm{I} = -10\mathrm{m/s}, v_\mathrm{O} = -15\mathrm{m/s}$
P_TX	20dBm
G	ideal cosine element (azimuthal direction)
σ	-3dB
ϑ	300K
$B_\mathrm{IF,ENBW}$	20MHz
F_N	10
f_0	$f_{0,\mathrm{I}} = 76.127\mathrm{GHz}, f_{0,\mathrm{V}} = 76\mathrm{GHz}$
k	$k_\mathrm{I} = 9.212\mathrm{MHz\mu s}$, $k_\mathrm{V} = 20.833\mathrm{MHz\mu s}$
T	$T_\mathrm{I} = 92.463\mu\mathrm{s}$, $T_\mathrm{V} = 48\mu\mathrm{s}$
N	$N_{\{\mathrm{V,IF}\}} = 1024$
M	$M_{\{\mathrm{V,IF}\}} = 128$

At every step, the following is done:

- Power levels are calculated according to (2.18) and (2.20). This can be seen on Fig. 2.17a. The noise floor stays constant while the powers of both interferer and object increase with a rate according to their approaching velocity. At the very last steps, there is a sudden decrease of interference power due to the interferer coming very close and therefore the angle between the radar beams becoming larger.

- Standard RD processing is applied. The result is illustrated in Fig. 2.17c, where the object peak and the *mean* noisefloor are separated and a range cross-section view is shown overlaid for every step (a Doppler view is essentially equivalent in the ramp-incoherent case). When comparing these signal magnitudes with the received power levels, a processing gain as in (2.23) can be observed. The object signal is amplified by roughly $10\log\left(\frac{512}{128}\right) = 48$dB, while interference is attenuated by about $10\log\left(\frac{5155}{131072}\right) = -14$dB .

- Finally, object peaks are detected. A CA (Cell Averaging) CFAR (Constant False Alarm Rate) object detector [47] was used. Here we see from Fig. 2.17b that the motorcycle can

only be reliably detected at a distance of $10 - 15$m. Naturally, there is a large number of possible algorithms/parameters to vary for the detector, which may change its performance. Nevertheless, this example shows that even with the large processing gain, interference can lead to a dangerous degradation of radar performance.

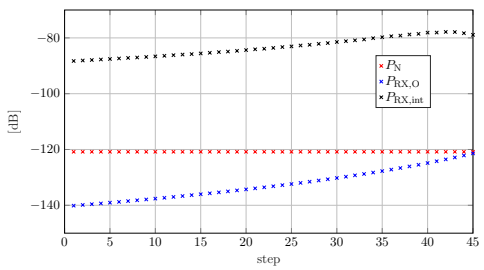

(a) Received powers

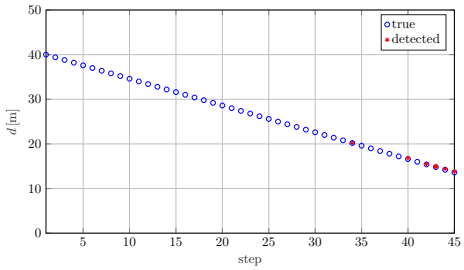

(b) Detections

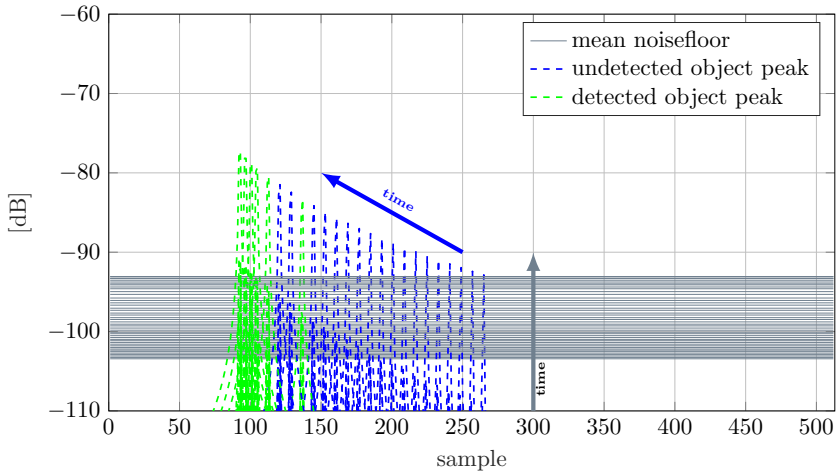

(c) RD map (range cross-section view)

Figure 2.17: Depiction of simulation outputs for the example scenario.

3 Discussion of Mitigation Methods

Chapter 1 introduced the signal processing framework for automotive FMCW/CS radar. Chapter 2 described the effects of (non-coherent) interference in the context of said signal processing. In this chapter, turning to the second fundamental topic of this work, methods to be embedded into the processing chain that can possibly mitigate interference will be discussed. Section 3.1 gives a classification and overview of the mitigation methods to be analyzed. Sections 3.2 to 3.7 describe each method separately.

3.1 Classification of Algorithms

The previous chapters were an attempt to give a concise description of interference, with some intent of simplifying the analysis and synthesis of mitigation algorithms. However, it is quite clear that the breadth of possible methods is very large and their performance, whether in some general sense or specific to certain cases, is not simple to predict in advance. Therefore first, the approaches dealt with in this thesis are introduced and categorized.

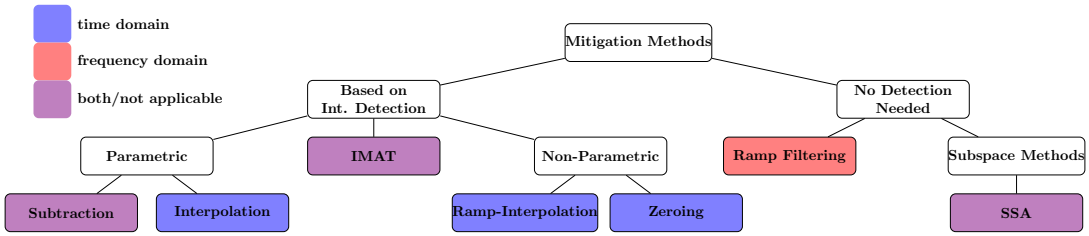

Figure 3.1: Classification of interference mitigation methods.

Fig. 3.1 shows a possible categorization of methods in a tree structure. In fact, a distinction of 4 dimensions of mitigation can be made.

- Dependence on interference detection – We can distinguish between algorithms that require exact knowledge about the location of interfered samples and those that do not.
- Mitigation in frequency or time domain – Methods might use the time domain IF signals $s_{\mathrm{IF}}^{(m)}(t)$ or the spectra after range compression $S_{\mathrm{IF}}^{(m)}(f)$.
- Mitigation in slow-time or fast-time – Some methods operate on the rows of the RD matrix, others on its columns.
- Parametric or non-parametric approach – Whether a parametric signal model is explicitly used in the design of the mitigation algorithm.

In the next sections, mitigation methods will be introduced in the context of these dimensions. The approaches dealt with in this thesis are listed below.

- Zeroing – The interfered samples are simply set to have a value of zero.

- (Ramp-)Interpolation – Interference bursts are replaced by a reconstruction of the non-interfered *object signal*.
- Subtraction – Samples impaired by interference are used to reconstruct the *interference signal*, which is then subtracted from the total received signal with the purpose of eliminating the interference component.
- Ramp Filtering – Recovery of object magnitude values based on a non-linear operation in slow-time domain over the range-compressed matrix $S_{\mathrm{IF}}^{(m)}(f)$.
- IMAT – Iterative sparse sampling method to recover the time domain object signal at a previously zeroed burst.
- SSA – An algorithm to adaptively transform the time domain signal into a signal basis in which interference and object components are separated. Components corresponding to objects are then chosen and transformed back into the time domain.

3.1.1 The Need for Explicit Detection

The first subdivision in Fig. 3.1 indicates whether an initial stand-alone detection step is needed prior to the actual mitigation process. Naturally, the majority of algorithms do need some detection, since they are based on the assumption of interference with specific properties.

An important exception is *ramp filtering*, where essentially the spectral diversity of ramps in a sequence is exploited. Since no assumption about interference is made except that it varies across ramps, the algorithm can be applied initially "blindly".

Another general approach not relying on prior detection is the decomposition of the received signals such that interference and object appear as more separate components in order to enable a simpler subsequent cancellation operation. Such *subspace methods* are heavily based on sophisticated signal theory, see *SSA (Singular Spectrum Analysis)*.

Concerning techniques requiring detection, a distinction to make is about the "resolution" of the decision.

- Detection of interfered ramps only: in particular for frequency-domain methods, it is only necessary to make a binary decision at every received ramp whether interference is present at all. Such information is useful even for other methods, since an efficient implementation only mitigates interference at the signals which are actually affected.
- Detection of interfered samples: for time-domain cancellation especially, the exact sample indices to be processed need to be known.

We are interested in the critical case of high interference power. This means that interferences in the time-domain IF signal appear as high-amplitude bursts (of varying duration, but shorter than the total ramp duration). Hence, a binary decision for a certain ramp can be assumed to be generally relatively simple, e.g., by analyzing the energy concentration/variance of the signal. In frequency-domain, interference is broadband, while a pure object signal is sparse, essentially a property dual to the time-domain, so that a similar measure can be used.

Naturally, if the time-domain interference burst needs to be localized accurately, the issue is somewhat more difficult, since it is not sufficient to only detect the presence of high-energy samples. All of the time-domain methods grouped into *Based on Detection* have this requirement. In particular, time-domain *subtraction* heavily relies on accurately finding the samples corresponding to a single burst.

3.1.2 Choice of Signal Domain

The input for a mitigation algorithm can be the signals prior to RD processing, as well as those of the range spectrum (after the first FFT). This grouping is indicated in Fig. 3.1 as the fill color of the rectangle, blue being the time- and red the frequency-domain. Purple indicates a method where either variants for both domains exist, e.g. *subtraction*, or where this grouping is rather ambiguous, e.g. *IMAT* which is an iterative procedure based on transformations between the two domains.

In addition to the time-frequency distinction, in the context of RD processing the notions of a fast-time and a slow-time domain arise. Naturally, it is also possible to develop a mitigation method that processes the slow-time signals, an example being *ramp filtering*, but also *ramp-interpolation*.

Therefore in total there are basically four options for the choice of signal domain. Although these are essentially different perspectives on the same phenomenon, the resulting differences in the signal properties of both object and interference lead to significant effects for mitigation considerations.

3.1.3 Usage of Parametric Model

The final important distinction is between algorithms that directly make use of a signal model, in contrast to those that only implicitly assume some signal properties (*ramp filtering*, *IMAT*), or indeed assume none at all (*zeroing*).

In the first case, the model can either be that of the object signal, essentially a sum of sinusoidals, as in the case of *interpolation* techniques, or a model of interference in the case of *subtraction*. Both of these are based on the problem of unknown parameter estimation. In general, parametric methods may achieve superior performance to non-parametric ones. However, for this, two conditions have to be met.

- The signal and noise models are accurate. This might be given for the object signal, provided we estimate from non-interfered samples. However, it is not always the case for interference, for example if symmetry is assumed.
- The estimation is accurate enough for the subsequent cancellation step. This can pose a problem in the case of *interpolation*, since the SNR (Signal-to-Noise Ratio) of the object signal might be quite low. For *subtraction*, while the "SNR" of interference is higher, accuracy requirements are as well, due to the parameter sensitivity of the model (see Section 2.2.5) combined with the nature of a subtraction operation.

In the following, the methods named in this section will be more exactly described and analyzed.

3.2 Zeroing of Interfered Samples

Setting the received samples that were affected by interference to zero is arguably the simplest, most obvious mitigation method. It has been discussed in e.g. [20], and often serves as a baseline of comparison to other methods [38], due to its ease of implementation in practical signal processors.

3.2.1 Implementation and Variants

The basic idea is

$$\tilde{s}_{\mathrm{IF}}[n] = \begin{cases} 0 \text{ for } n \in \mathcal{N}_{\mathrm{int}} \\ s_{\mathrm{IF}}[n] \text{ otherwise} , \end{cases} \tag{3.1}$$

where $\mathcal{N}_{\mathrm{int}}$ represents the indices of the samples affected by interference. As a generalization, for a continuous burst of interference with a center sample at $n_{\mathrm{int,c}}$ and length N_{int}, one can write

$$\tilde{s}_{\mathrm{IF}}[n] = s_{\mathrm{IF}}[n] w_{\mathrm{inv},N_{\mathrm{int}}}[n - n_{\mathrm{int,c}}]. \tag{3.2}$$

Here, $w_{\mathrm{inv},N_{\mathrm{int}}}[n - n_{\mathrm{int,c}}]$ is an inverse window of the appropriate length and shift, and hence the technique is known as *inverse windowing*. If a rectangular window is chosen, this becomes the simple zeroing operation as in (3.1). A more detailed description can be found in [20] .

3.2.2 Properties

The previous section left out the initial step of detecting interference and therefore determining $\mathcal{N}_{\mathrm{int}}$. For this mitigation technique, detection is however the most crucial step, since the subsequent operation is trivial.

In any case, assuming perfect detection, zeroing has the ability to completely eliminate interference. This is in fact different from other methods, and makes zeroing not well defined in terms of an analysis of SINR gain. Rather, the effect of this method on the remaining object signal is to be discussed, since this method completely eliminates a part of the signal, thus also neglecting useful information. Essentially, the loss of samples leads to a loss of spectral resolution, and hence a decreased localization of object peaks on the RD map. This is qualitatively illustrated in Fig. 3.2.

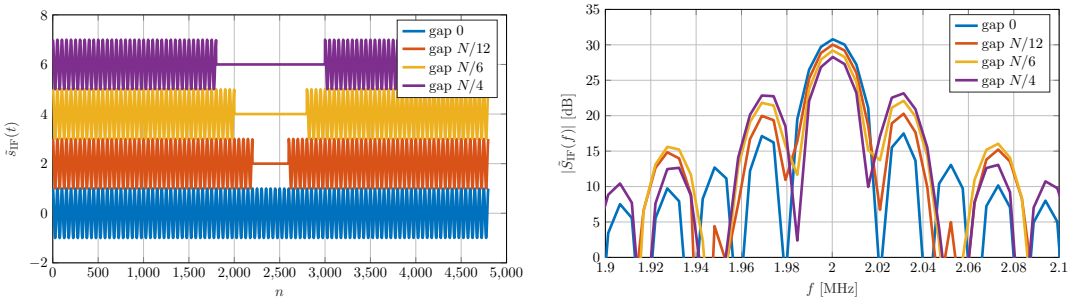

(a) Time-domain signals. *(b) Frequency magnitude spectra.*

Figure 3.2: Simple example where a gap of variable length inside an object signal is set to zero. An offset to the time domain signals was added only for visualization purposes.

3.3 Time Domain Interpolation Methods

Interpolation methods have been mentioned as early as in [14] . Similar to zeroing, they are based on the detection of interfered samples. However, these samples are then replaced ("gaps" are interpolated) with the intent of reconstructing the clean object signal. This can be done through the use of a signal model estimated from the remaining non-interfered data, or by some other interpolation technique.

3.3.1 Implementation and Variants

In a very general form, the mitigation output is given by

$$\tilde{s}_{\mathrm{IF}}[n] = \begin{cases} \hat{s}_{\mathrm{IF}}[n] = g(s_{\mathrm{IF}}[n\pm1]...s_{\mathrm{IF}}[n\pm L]) \text{ for } n \in n_{\mathrm{int}} \\ s_{\mathrm{IF}}[n] \text{ otherwise} , \end{cases} \tag{3.3}$$

where $g()$ is some interpolation function of the signal at (negative or positive) lags $1...L$.

Linear Prediction and a Parametric Approach

A linear prediction problem can be considered,

$$\hat{s}_{\mathrm{IF}}[n] = \sum_{l=1}^{\eta} a_l s_{\mathrm{IF}}[n-l], \tag{3.4}$$

where η is the model order and a_l the prediction coefficients. The crucial point is the choice of the prediction coefficients, which could be calculated using signal modeling knowledge. One of the natural options is an AR (AutoRegressive) model. However, in this thesis, a slightly different approach based on [48] is attempted. It has not been directly used for interference mitigation previously.

In [48] , it is shown that for a sum of sinusoidals, a unique set of coefficients satisfying (3.4) exists for $\eta = 2\times$(Number of Sinusoidals). Afterwards, the noise model is incorporated, and the prediction is written as a system of linear equations for $N_{\mathrm{est}} > 2\eta$ measurements (samples). A least-squares estimate of the equation coefficients a_l can then computed using the IVM (Instrumental Variable Method) [49], with the instrumental variable being simply the input matrix delayed by some value, termed Δ, in order to ensure uncorrelatedness. Essentially, IVM consists of an estimation step

$$\hat{\boldsymbol{a}} = (\boldsymbol{Z}^T \boldsymbol{X})^{-1} \boldsymbol{Z}^T \boldsymbol{y} \tag{3.5}$$

where

$$\boldsymbol{y}^{\mathrm{T}} = \begin{bmatrix} s_{\mathrm{IF}}[2\eta+1] & s_{\mathrm{IF}}[2\eta+2] & \dots & s_{\mathrm{IF}}[N_{\mathrm{est}}] \end{bmatrix} \tag{3.6}$$

$$\boldsymbol{X} = \begin{bmatrix} s_{\mathrm{IF}}[2\eta] & \dots & s_{\mathrm{IF}}[1] \\ s_{\mathrm{IF}}[2\eta+1] & \dots & s_{\mathrm{IF}}[2] \\ \vdots & & \vdots \\ s_{\mathrm{IF}}[N_{\mathrm{est}}-1] & \dots & s_{\mathrm{IF}}[N_{\mathrm{est}}-2\eta] \end{bmatrix} \tag{3.7}$$

$$\boldsymbol{Z}^{\mathrm{T}} = \begin{bmatrix} s_{\mathrm{IF}}[2\eta+\Delta] & s_{\mathrm{IF}}[2\eta+\Delta+1] & \dots & s_{\mathrm{IF}}[N_{\mathrm{est}}+\Delta-1] \\ s_{\mathrm{IF}}[2\eta+\Delta+1] & \dots & \dots & s_{\mathrm{IF}}[N_{\mathrm{est}}+\Delta] \\ \vdots & & & \vdots \\ s_{\mathrm{IF}}[4\eta+\Delta-1] & \dots & \dots & s_{\mathrm{IF}}[N_{\mathrm{est}}+2\eta+\Delta-2] \end{bmatrix}, \tag{3.8}$$

followed by the interpolation step as in (3.4). Note that in fact only $\eta+1$ out of the 2η coefficients are unique, and hence we can use a constrained version of the algorithm to achieve better performance; the corresponding equations can be found in [48] .

An outline of the algorithm as implemented in simulation can be described as:

1. Determining which samples are interfered.
2. Using one or several non-interfered ramps or signal parts, (3.4) – (3.6) are implemented. The choice of the number of estimation samples N_{est} can be set in a trade-off between

estimation accuracy and computational efficiency.

3. At the interfered ramps, bursts of impaired samples are interpolated by (at each sample, respectively) applying (3.3), starting at the edge of the interfered burst. Optionally, the interpolation result is normalized by the object signal power estimated from "clean" samples previously, to ensure amplitude consistency.

Figure 3.3 illustrates the application of the algorithm on an interference burst in one of the received ramps. The simulation assumes perfect detection, although the exact limits of the burst are slightly washed out due to a simulated AAF. $N_{\text{est}} = 1000$ non-interfered samples were used to compute a_l. The signal stems from a single object, so that $\eta = 2$. As it can be seen, there is a mismatch in the phase (and amplitude) of the reconstructed signal when compared to the original. Nevertheless, the general validity of the model is easily recognized.

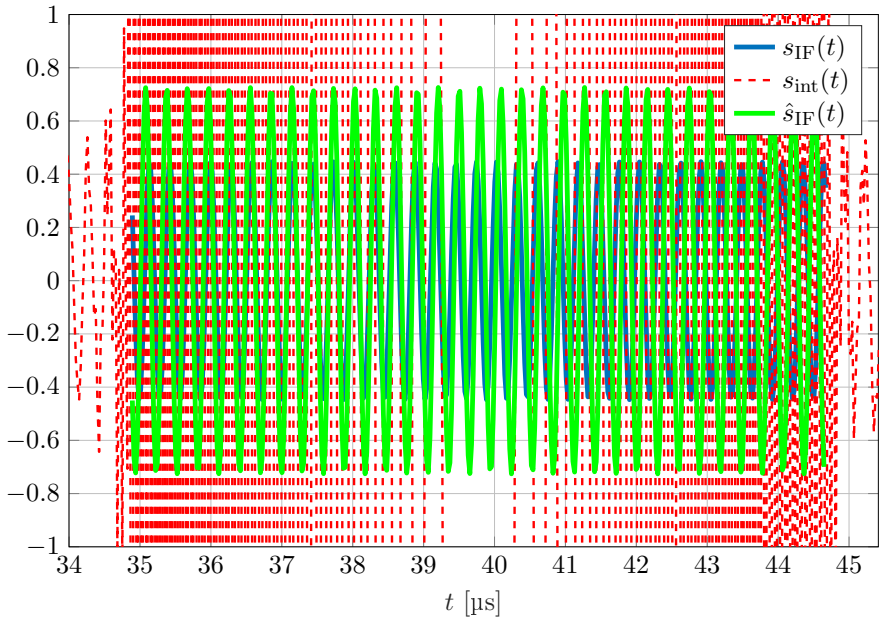

Figure 3.3: Example of interpolation result using the proposed IVM-based method.

Linear Interpolation in Ramp-Domain

A simple non-parametric approach is to compute a linear interpolation

$$\hat{s}_{\text{IF}}[n] = (s_{\text{IF}}[n-1] + s_{\text{IF}}[n+1])/2, \tag{3.9}$$

essentially a weighted average with coefficients $\boldsymbol{a} = [1/2\ 1/2]$. (Note that this could be generalized as the averaging of any number of neighboring samples.)

In the fast-time domain, where interference is a burst of several (possibly hundreds of) samples, such a naive technique is rather ineffective. However, if interference density in a measurement is reasonably low, interference in slow-time might appear as single interfered samples surrounded by non-interfered ones. In this case, a crude assumption of linearity might be possible to make.

Fig. 3.4 shows the results of such an approach for a single object sinusoidal, illustrated the same way as for the prediction approach in Fig. 3.3. For the set input noise power with SNR = 10dB, the processed signal can be seen to "follow" the original sine quite well.

A parametric method, such as the one discussed in the previous subsection, could in principle be also used in the slow-time domain. The signal model is a sum of sinusoidals here, as well.

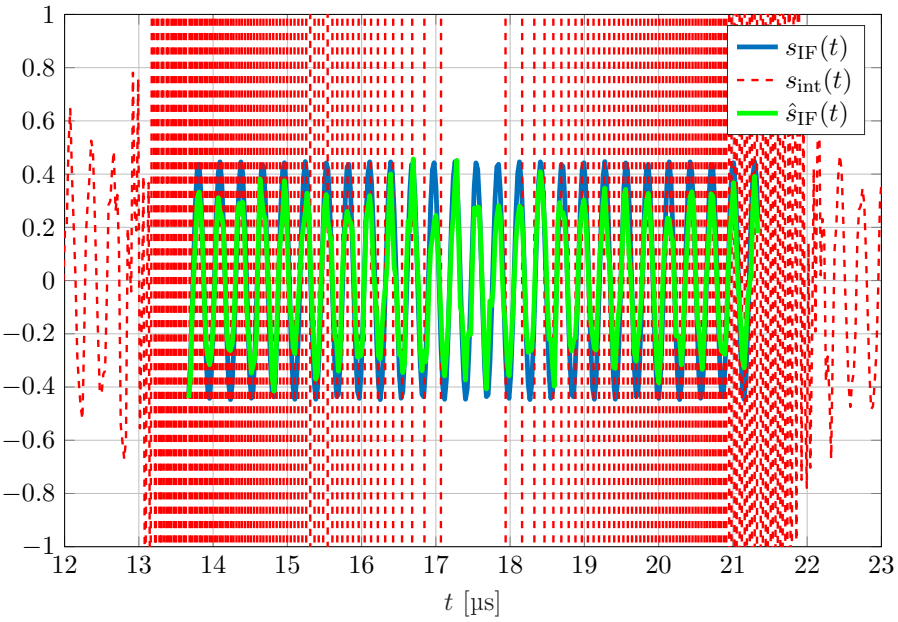

Figure 3.4: Example of interpolation result using the proposed slow-time linear interpolation method.

Another option that should be mentioned is that linear interpolation could be changed to e.g. a higher-order polynomial interpolation technique, promising a possibly better performance while increasing computational complexity.

3.3.2 Properties

The method of interpolation can be thought of as a generalization of zeroing, since interference samples are detected and then replaced. Hence, just as discussed in Section 3.2.2, sample detection performance is crucial, and interference itself is eliminated completely in the case of perfect detection. However, in contrast to zeroing, the intent is to replace interference by a "meaningful" component. This leads to a danger in these methods, since it can in principle cause components to appear and possibly be detected as objects that were in fact not part of the original receive signal. Such an effect is of course to be avoided for any practical implementation.

Crucial for the IVM-based method in this context is the model order η, since it sets the number of spectral peaks the algorithm tailors its estimation to. In the example presented in Fig. 3.3, η has been generously set to the correct value. However in practice, the number of components naturally is never known in advance. In this case, a model order-recursive implementation [50] is needed, the robustness of which is yet to be determined in the future.

Another aspect, worth noting for parametric variants, is that an estimation such as (3.5) is essentially already a (relatively sophisticated) attempt at determining the objects' frequency components. The purpose of interference mitigation generally, however, would be rather to *efficiently* preprocess the signal for subsequent detection of objects on the RD map. In terms of efficiency, such estimation-based methods are rather computationally demanding.

Observing (3.6), to increase performance we might use a large number of samples N_{est}, which leads to multiplications and the inverse operation needing to be done on large matrices. It is, however, possible to use a recursive form of the algorithm. In addition, a single computation of a (using e.g. samples in one ramp known to not contain interference) per measurement should be sufficient; only the phase changes between ramps, which has no effect on the correct values of the required interpolation coefficients.

Concerning linear interpolation, it can be said that it is simple to compute and hence well-

suited as a quick pre-processing step. It also does not carry much danger in terms of the creation of false objects, provided only units of single samples are replaced. In addition, it is essentially independent of the actual number of objects present. However, no high performance can be expected either, in terms of the variance of the estimate provided by (3.9) at low SNR. At practical slow-time signal lengths, the assumption of local linearity is rather inaccurate, as well.

3.4 Estimation and Subtraction of Interference Signal

Subtraction is in some sense the "dual" of interpolation. It does not use knowledge on the object signal, but on interference, and tries to approximate its component in the receive signal. Since interference is assumed to be additive (and is a deterministic signal), we can in principle simply subtract a proper approximation to regain a non-interfered object signal. Such a *cancellation* (another term used for substraction) algorithm based on the symmetric time-domain interference burst form has been proposed in [36] and [37]. Additionally, a novel frequency-domain subtraction approach is briefly introduced in this work.

3.4.1 Implementation and Variants

The basic operation is

$$\tilde{s}_{\mathrm{IF}}[n] = \begin{cases} s_{\mathrm{IF}}[n] - \hat{s}_{\mathrm{int}}[n] \text{ for } n \in n_{\mathrm{int}} \\ s_{\mathrm{IF}}[n] \text{ otherwise} , \end{cases} \tag{3.10}$$

where $\hat{s}_{\mathrm{int}}[n]$ is some estimate of the interference component. Consequently, the key performance point for this family of methods is how to obtain said estimate.

Time-domain phase and amplitude estimation

It was shown in Section 2.1 that a single burst of interference can be described by a chirp, meaning a sinusoidal with a certain envelope and a quadratic phase course. In the case of a complex (I/Q) received signal, said phase course is directly embedded as the complex phase of the corresponding samples.

In [37], a method of first estimating the phase and subsequent least-squares approximation of a constant amplitude is introduced. It is derived in continuous-time, for the complex signal, making use of the approximation that the time-derivative of the received signal is strongly dominated by the interference component. Then, a phase estimate is given simply by, using the real parts of the signals,

$$\hat{\varphi}_{\mathrm{int}}[n] = \tan^{-1}\left(-\frac{\Re\{\frac{\mathrm{d}}{\mathrm{d}t} s_{\mathrm{IF}}[n]\}}{\Im\{\frac{\mathrm{d}}{\mathrm{d}t} s_{\mathrm{IF}}[n]\}} \right), \tag{3.11}$$

which can be discretized through the use of the difference quotient as a derivative. Following that, the amplitude is computed by

$$\hat{A}_{\mathrm{int}} = \frac{\sum \cos(\hat{\varphi}_{\mathrm{int}}[n]) \Re\{s_{\mathrm{IF}}[n]\}}{\sum \cos(\hat{\varphi}_{\mathrm{int}}[n])^2}. \tag{3.12}$$

Finally, (3.10) can be carried out, with

$$\hat{s}_{\mathrm{int}}[n] = \hat{A}_{\mathrm{int}} \cos\left(\hat{\varphi}_{\mathrm{int}}[n]\right). \tag{3.13}$$

Note that this process is for a single interference burst. Concerning a real-only input, in [37] it is stated that the method can be effectively applied in that case, as well, using a Hilbert transform first to obtain the corresponding complex signal.

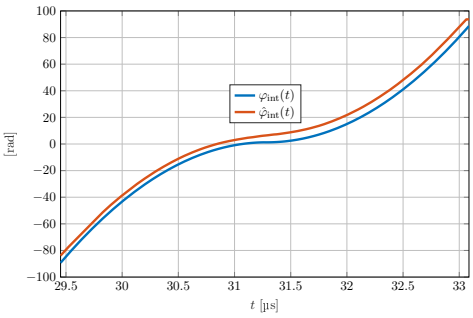

(a) Original and estimated phase of an interference burst.

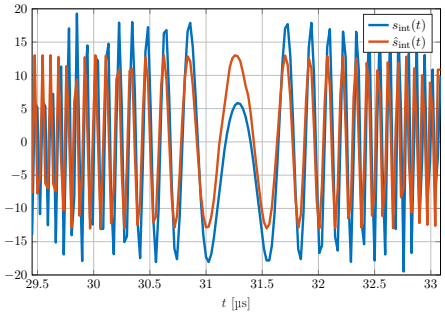

(b) Original and estimated interference signal.

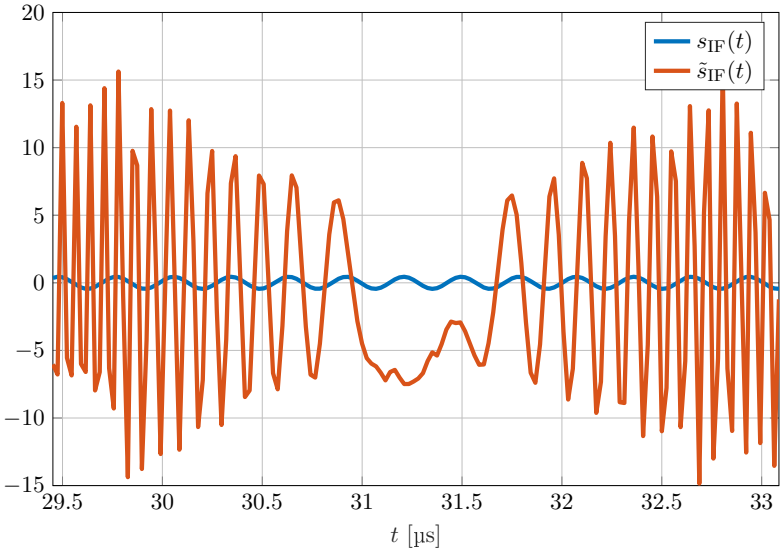

(c) Clean object signal compared to the result of subtraction.

Figure 3.5: Example of estimation and subtraction results using the described time domain method.

In Fig. 3.5, the simulation result of applying the algorithm to an interfered signal is plotted. First, the phase is depicted in Fig. 3.5a. Note that the first half of φ_{int} has been inverted and an absolute phase offset corrected for an easier visual comparison to $\hat{\varphi}_{\text{int}}$. Fig. 3.5b then shows the original interference signal and the one estimated via (3.11) and (3.12). Lastly, in Fig. 3.5c we see the clean object signal together with the result of the subtraction operation as (3.10).

We can observe that while the estimated phase follows the original one generally well, non-ideal estimation leads to a (non-constant) phase offset. The error is largest around $f = 0$, as is also mentioned in the cited reference. In addition, the AAF used in simulation to introduce a degree of realism results in a non-constant envelope. This somewhat compromises the amplitude estimation technique. The accumulation of moderate estimation errors, together with the sensitivity of the subtraction operation, lead to a significant amount of interference remaining on Fig. 3.5c.

Frequency-domain technique

Eq. (3.10) can in principle also be implemented in the frequency-domain, on the range spectra. A difference is that interference is not (well) localized in frequency. Therefore, basically an estimation of magnitude and phase over the whole bandwidth is to be made. This is generally not a simple task due to the unknown interference parameters resulting in a complicated magnitude spectrum form.

In case of a complex receiver, however, there are key properties of the range spectrum that can be exploited.

- Objects appear as peaks of *positive frequencies only*.
- In the symmetric interference burst case, it holds for the interference magnitude spectrum that

$$|S_{\mathrm{int,IQ}}(f)| = |S_{\mathrm{int,IQ}}(-f)|. \tag{3.14}$$

  This was also illustrated in Fig. 2.3.

- Similarly for the phase, it holds that

$$\phi_{\mathrm{int,IQ}}(f) \approx \phi_{\mathrm{int,IQ}}(-f) + 2\pi f 2\tau_{\mathrm{int}}. \tag{3.15}$$

Equations (3.14) and (3.15) directly follow from the considerations made in Section 2.2.4. A possible interference mitigation technique is then to compute for the positive frequencies $f > 0$

$$\tilde{S}_{\mathrm{int,IQ}}(f) = S_{\mathrm{int,IQ}}(f) - |S_{\mathrm{int,IQ}}(-f)|\mathrm{e}^{\mathrm{j}2\pi f 2\hat{\tau}_{\mathrm{int}}}. \tag{3.16}$$

This operation exploits the symmetry in the magnitude spectrum to ideally cancel the interference component at the positive frequencies (where the object peaks are located). An estimation of a phase parameter is still required, tough.

The approach has not been proposed before. It is relatively simple, and might be effective if a complex receiver is available. However, the algorithm has not yet been extensively tested in a practical implementation. Therefore, more research is to be done in the future.

3.5 Ramp Filtering

The concept of ramp filtering was introduced in [39]. It offers a significantly different approach to the previously discussed methods, yielding unique advantages. The main idea is not to directly attempt to mitigate interference at the affected ramps/samples, but to exploit the diversity of the range spectrum in ramp domain.

3.5.1 Implementation and Variants

The basic approach to ramp filtering as described in [39] is limited to mitigation of interference in the *magnitudes* of the RD matrix after the first FFT.

The ramps of said matrix are processed by some nonlinear operator $g()$, which can be written in the most general form as

$$\tilde{S}_{\mathrm{IF}}^{(m)}[n] = g\left(\begin{bmatrix} S_{\mathrm{IF}}^{(1)}[n] & \dots & S_{\mathrm{IF}}^{(M)}[n] \end{bmatrix}\right), \tag{3.17}$$

where the superscript in parentheses denotes the ramp index in this case.

The choice of nonlinear operator is of course a significant aspect influencing the characteristics and performance of the algorithm. The concept itself allows for many possibilities.

A natural choice is the minimum operator min(). At range bins where no object is present, this takes the value of smallest interference/noise power. At ranges where an object is located, it is a component in every ramp. Although the behavior is not deterministic, by taking the minimum, the resulting magnitudes should be very small at every point other than the object bins, improving ranging SNR considerably.

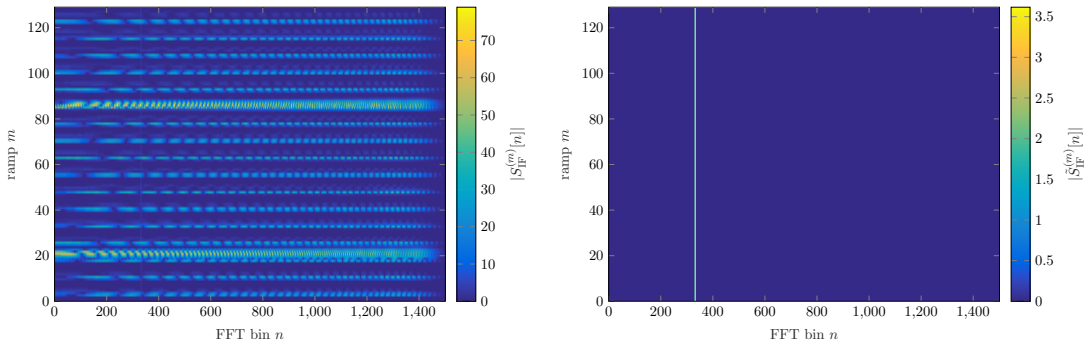

(a) Input magnitude matrix to the algorithm. *(b) Mitigation result.*

Figure 3.6: Example of magnitude correction based on the values of the first FFT at the ramps.

On Fig. 3.7, the interfered matrix together with the result of magnitude processing is visible. While $S_{\mathrm{IF}}^{(m)}[n]$ is strongly interfered for many of the ramps m, several ramps are not affected, as well. The global minimum over the ramps yield a single range spectrum of length N. This is then simply copied M times to reconstruct a matrix of the original size. The result is a matrix with a single visible "ridge" corresponding to the object.

However, only magnitude values are changed this way. For the phase values, it is the change across ramps that encodes the resulting velocity information for the objects. This means (3.17) cannot simply be implemented. A method has been proposed based on the reconstruction of the object phase using the ramps that are not interfered, which will be briefly described next.

Phase Correction

The proposed phase correction, although used as an addition to ramp filtering, is in fact a parametric interpolation approach. This makes it technically a part of the family of interpolation methods as discussed in Section 3.3. It relies on the fact that a single object has linear phase over the slow-time samples (at the range bin it occupies), see Section 1.1.1.

The method requires the identification of frequency bins corresponding to objects, as well as of ramps that are not (significantly) interfered. The former can be done using the range spectrum obtained by an assumed successful magnitude correction. The latter is needed because with very strong interference, the sensitive phase of the object is distorted to a degree such that it cannot be used in the interpolation scheme. It can be implemented using, e.g., some relative spectral energy criterion (the issue of detection has already been briefly discussed in Section 3.1.1).

The detected, non-interfered slow-time samples at an object bin are then used to estimate the parameters of a linear function. Using that, the phase course is reconstructed by interpolation of the interfered samples.

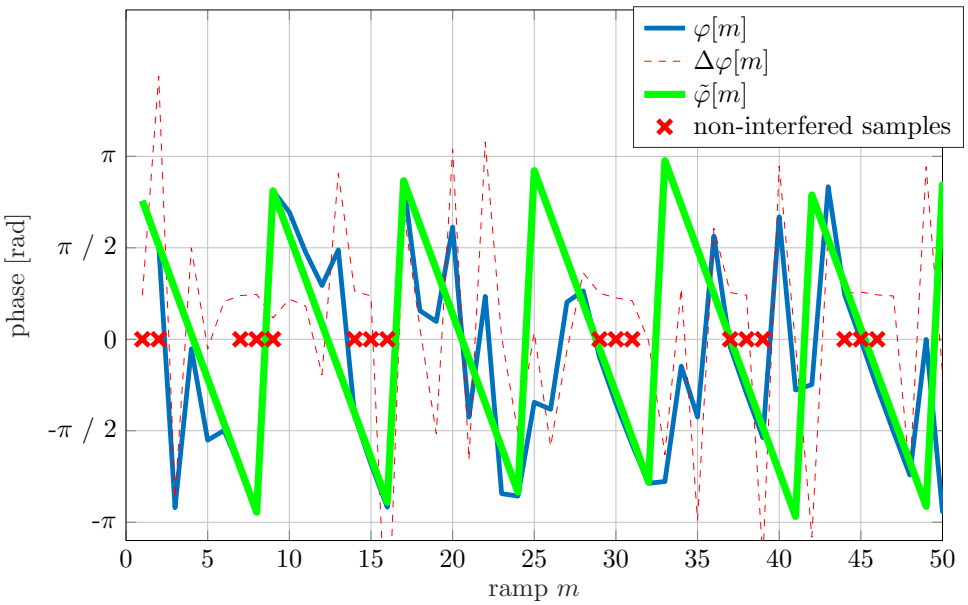

Figure 3.7: Example of phase processing at an object bin.

Fig. 3.7 shows the application of the phase processing subsequent to the magnitude ramp filtering as already shown for the example in Fig. 3.6. Through the use of the numerical derivative at non-interfered phase values $\Delta\varphi[m]$, a simple estimate for the slope is obtained. The phase values at interfered samples are then interpolated. Other, more sophisticated estimation techniques are possible; however, the described method has the significant advantage of computational simplicity.

3.5.2 Properties

The correction of magnitudes as originally proposed is the practically simplest method discussed in this work so far. A big advantage is that no detection is needed, and neither is anything assumed about the signal model of interference, leading to considerable efficiency and flexibility. One assumption the method makes is the diversity of interference in ramps. In particular, using the minimum operator is effective due to the assumption of at least one "good" ramp present in the measurement.

The two main disadvantages of this method are as follows. First, it discards the phase values, for which the additional phase correction technique is needed. Second, it is difficult to guarantee a certain behavior of the nonlinear operation. As an example, let us consider using the minimum operator on the magnitude values. Note that these are a result of the complex sum of objects and interference. Therefore it is very much possible at one of the ramps for interference to cause the resulting object bin magnitude to be very small, which the operator would then choose, yielding a very low SNR.

The phase correction method is relatively simple, as well, and has a good performance provided the number of "good" ramps is relatively high. However, it does not work in the case of several objects within the same range bin with different velocities, since then the phase course over the ramps is not a simple linear function anymore. Additionally, to correct the phase, detection becomes a necessity, somewhat negating the advantage of the initial magnitude filtering.

Variations in the behavior of the algorithm are very large, depending on the choice of filter for the magnitude and the detection criteria for the subsequent phase correction. Further research is necessary to explore these dynamics. One option to consider, for instance, is to first discard ramps in which the spectrum is highly dominated by interference, and process only the remaining

ones.

3.6 Iterative Method with Adaptive Thresholding

IMAT was introduced in the context of sparse sampling in [51]. The idea was then used for a novel interference mitigation approach in [38].

3.6.1 Implementation and Variants

The method is proposed to be used per (interfered) ramp, on the fast-time samples. A prerequisite for the method is an initial detection and zeroing step. This ensures, provided not too many samples are zeroed, that the spectrum of the signal is sparse. Sparsity essentially means that spectral energy is concentrated around a relatively small number of components.

The concept is to interpolate the zeroed time-domain gap by iteratively finding said dominant components in frequency domain and replacing the gap by their inverse Fourier transform. At every step, the discontinuity and hence spectral resolution loss associated with the zeroing method is decreased.

The extraction of dominant components is done by thresholding, starting with taking only the maximum value (strongest spectral peak), and then lowering the threshold at every iteration by $\Delta\,\mathrm{dB}$. This step size, together with the number of iterations to make $\eta_{\max}$, are the parameters of the algorithm. In [38], a way to determine appropriate values for the parameters is given. However, in general, as long as spectral sparsity can be assumed and the threshold does not get set below the noise floor, IMAT can be applied.

Fig. 3.8 illustrates the effectiveness of the algorithm. While the initial zeroing suppresses the noise, it leads to the two object peaks not being distinctly detectable. It can be observed that IMAT then performs a step-wise reconstruction of the components.

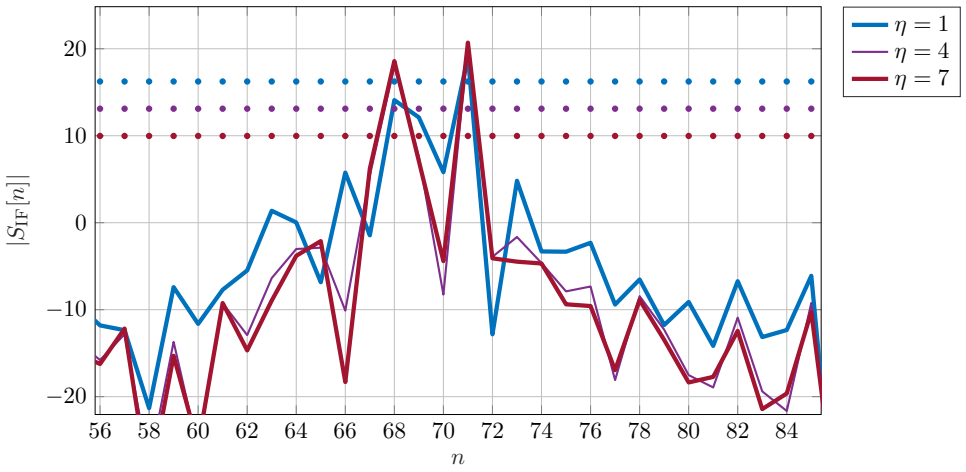

(a) Magnitude spectrum at different steps of thresholding.

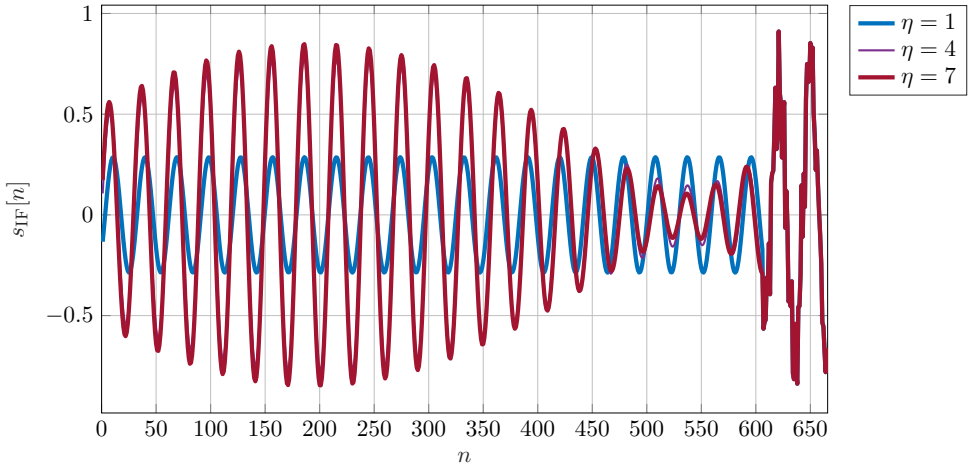

(b) Corresponding time domain signal at the reconstructed gap.

Figure 3.8: Application of IMAT in an example simulation with strong interference and two closely spaced objects. The iteration index is termed η. Dotted lines symbolize the threshold levels.

3.6.2 Properties

The method is conceptually simple and does not require assumptions about the nature of the interference, since it is an addition to zeroing. It attempts to have the advantage of interference noise reduction provided by zeroing while reducing the loss in resolution caused by it. It can certainly improve on the performance of pure zeroing in this way. One aspect of IMAT worth noting is its computational requirements; per interfered ramp, $2\eta_{\max}$ transformations (FFT and IFFT (Inverse FFT)) are needed.

3.7 Singular Spectrum Analysis

SSA is an established technique for non-parametric time-series analysis [52]. It has been used in many applications, e.g. [53]. A concept to use SSA for interference mitigation has been proposed.

Omitting an exact exploration of its mathematical background, the basic idea is to decompose the signal into a number of independent components, just like in any signal transform. However, the basis for the transform is computed adaptively, making use of the inherent structure of the data itself. Decomposition can then be followed by a decision step, where the components

deemed to correspond to noise are discarded. The remaining components can then be used to reconstruct the corresponding parts of the sequence in the original domain (analogous to an inverse transform).

3.7.1 Implementation and Variants

SSA processing can be applied per (interfered) ramp. The input to the algorithm is therefore the time domain sequence of length N, $s_{\mathrm{IF}}[n]$. The first step is to construct the so-called *trajectory matrix* $\boldsymbol{X}$. This is a matrix whose rows consist of lagged windowed versions of $s_{\mathrm{IF}}[n]$ in the following way:

$$\boldsymbol{X} = \begin{bmatrix} s_{\mathrm{IF}}[1] & s_{\mathrm{IF}}[2] & \dots & s_{\mathrm{IF}}[L] \\ s_{\mathrm{IF}}[2] & s_{\mathrm{IF}}[3] & \dots & s_{\mathrm{IF}}[L+1] \\ \vdots & \vdots & \vdots & \vdots \\ s_{\mathrm{IF}}[N-L+1] & s_{\mathrm{IF}}[N-L+2] & \dots & s_{\mathrm{IF}}[N] \end{bmatrix}. \tag{3.18}$$

This process is also called *embedding*. As can be seen on (3.18), the window is rectangular and of length L, L being the only input parameter to the algorithm that needs to be set in advance. The result $\boldsymbol{X}$ is hence of size $(N - L + 1 \times L)$.

The basis vectors of the adaptive transform are then the eigenvectors of the *covariance matrix*, which can most simply be obtained from the trajectory matrix by

$$\boldsymbol{C}_{XX} = \frac{1}{\sqrt{L}} \boldsymbol{X}^{\mathrm{T}} \boldsymbol{X} \tag{3.19}$$

$$= \boldsymbol{U} \boldsymbol{\lambda} \boldsymbol{U}^{\mathrm{T}}, \tag{3.20}$$

where $\boldsymbol{U}$ is a matrix containing the eigenvector of $\boldsymbol{C}_{XX}$, $\boldsymbol{u}_k, k \in [1..L]$, in its k-th column, and $\boldsymbol{\lambda}$ is a diagonal matrix formed by the eigenvalues λ_k.

The decomposition of the signal is then done by projecting the rows of the trajectory matrix on the eigenvectors, yielding the so-called *principal components* $\boldsymbol{p}_k$

$$\boldsymbol{p}_k = \boldsymbol{X} \boldsymbol{u}_k \tag{3.21}$$

In order to reconstruct the original sequence, for a given component we first determine the matrix $\boldsymbol{R}_k$ as

$$\boldsymbol{R}_k = \boldsymbol{p}_k \boldsymbol{u}_k^{\mathrm{T}}. \tag{3.22}$$

The corresponding time domain N-sample sequence $\tilde{s}_{\mathrm{IF},k}[n]$ can then be reestablished from R_k by, for every given $n = i$, computing the average of the i-th *antidiagonal* of R_k.

A subset of the components, termed $\mathcal{R}$ here, is chosen as the ones to be "kept" for the reconstruction step, so that the denoised time domain sequence resulting from the algorithm is

$$\tilde{s}_{\mathrm{IF}}[n] = \sum_{k \in \mathcal{R}} \tilde{s}_{\mathrm{IF},k}[n]. \tag{3.23}$$

This concludes an outline of the technique. For more detailed discussions, the reader may refer to the references cited above.

Choice of Components

Of course, determining $\mathcal{R}$ properly is critical to a satisfactory denoising performance. In particular, the choice of relevant signal components should be automatic and adaptive, making use

of some robust, reliable metric. In basic SSA, this is done simply by observing the eigenvalues of the covariance matrix. The values of λ_k essentially correspond to a measure of the signal energy in a certain decomposition component. It is then assumed that useful signals are concentrated (i.e., separated) into a relatively low number of single very high energy components. As a consequence, components corresponding to small eigenvalues can be discarded.

However, the previous reasoning is only correct, strictly speaking, if noise is uncorrelated (i.e., spectrally white). It is only in that case true that noise energy is spread across all components, independently of the signal basis. As we have seen in the previous chapters, however, interference possesses a certain deterministic structure. This structure is then "caught" by the process of constructing the signal basis, leading to a small number of strong components representing interference. Hence, even though the two become possibly very well separated, it is more difficult to tell an object signal and an interference component apart by just analyzing the eigenvalues.

Instead, remembering the typical burst-like nature of interference, a *time concentration criterion* was introduced. The measure C_k is computed on the component-wise time domain reconstructed signals $\tilde{s}_{\mathrm{IF},k}[n]$ so that

$$C_k = \frac{\sum_{n=1}^{N} |\tilde{s}_{\mathrm{IF},k}[n]|^2}{\left(\sum_{n=1}^{N} |\tilde{s}_{\mathrm{IF},k}[n]|\right)^2}. \tag{3.24}$$

This measure is large for signals that are concentrated in the time domain. $\mathcal{R}$ can therefore be determined accordingly.

3.7.2 Properties

The adaptivity of the signal transform implemented in SSA means that dominant signal components may be separated more clearly when compared to a non-adaptive transform. Nonlinearities can also be better "resolved", as opposed to e.g. Fourier analysis, which by definition projects the signal onto a basis of single-frequency oscillations only. We see this on the remarkable ability of the method to separate components of object signal, interference and noise in the decomposition. Other signal impairments could also in principle be separated, leaving the method flexible for environments different to the one we have been concerned with in this thesis.

As has already been mentioned, the crucial part of the method in which a somewhat arbitrary choice has to made is the measure by which the set of relevant components is found. With the time concentration criterion, an assumption about the structure of signal components is indeed made in advance. In addition, the input parameter L must be set. Nevertheless, in general it can be said that SSA is able to provide superior performance to simpler non-parametric methods while being significantly more flexible than parametric ones.

An aspect of the algorithm that makes any practical implementation within today's sensor signal processing hardware very difficult is its very high computational cost. There are several matrix operations involved, on matrices that are quite large. The process then has to be repeated for every interfered ramp accordingly.

4 Comparative Analysis of Techniques

In Chapter 3, the most important approaches to interference mitigation were introduced. It could be seen that there are several aspects in which algorithms can differ, and methods generally have their own unique properties. Nevertheless, we need to compare all these techniques in a meaningful way. This requires the definition of a metric by which methods can be ranked. Section 4.1 defines these performance measures, which are then used in Monte Carlo simulations for a comparison of mitigation techniques in Section 4.2. A brief description on the usage of measurement data for testing mitigation algorithms is given in Section 4.3. Finally, the most important findings are summarized in Section 4.4.

4.1 Definition of Performance Measures

Since objects in CS radar are detected as peaks on the RD map, there are two fundamental aspects relevant to the sensor's performance for a single object:

1. *Detection probability:* dependent on the SINR, meaning the magnitude of the peak compared to the noise floor. Note that the two dimensions of the RD matrix, corresponding to range and velocity, can exhibit a different SINR.

2. *Determination of detected object properties:* correct location of the peak on the RD map, object resolution capability ("width" of the peak), phase value (relevant for MIMO processing). Naturally, the ground truth needs to be known in order to evaluate this performance.

Essentially, the goal of interference mitigation preprocessing is to maximize detection probability (point 1) while avoiding any distortion possibly skewing the detection results (point 2). Based on this, and maintaining the view of a single object scenario only, the following numerical measures can be defined:

- SINR in range dimension, computed as

$$\mathrm{SINR_r} = \frac{\sum_{n\in\mathcal{O}} \left|S_{\mathrm{IF}}^{(m_\mathrm{O})}[n]\right|^2 / N_\mathcal{O}}{\sum_{n\notin\mathcal{O}} \left|S_{\mathrm{IF}}^{(m_\mathrm{O})}[n]\right|^2 / (N - N_\mathcal{O})}. \tag{4.1}$$

- SINR in velocity dimension, similarly

$$\mathrm{SINR_v} = \frac{\sum_{m\in\mathcal{O}} \left|S_{\mathrm{IF}}^{(m)}[n_\mathrm{O}]\right|^2 / M_\mathcal{O}}{\sum_{m\notin\mathcal{O}} \left|S_{\mathrm{IF}}^{(m)}[n_\mathrm{O}]\right|^2 / (M - M_\mathcal{O})}. \tag{4.2}$$

- EVM (Error Vector Magnitude), as measured between the complex values of the object peak in the non-interfered and mitigation processed cases,

$$\mathrm{EVM} = \frac{|S_{\mathrm{IF}}^{(m_\mathrm{O})}[n_O] - \tilde{S}_{\mathrm{IF}}^{(m_\mathrm{O})}[n_O]|}{|S_{\mathrm{IF}}^{(m_\mathrm{O})}[n_O]|}. \tag{4.3}$$

Table 4.1 explains the variables of the equations above. To simplify notation, $\mathcal{O}$ was introduced as the set of object samples, pertaining to both range and velocity. The definition of this set is somewhat arbitrary. Naturally, the actual maximal peak value is $S_{\mathrm{IF}}^{(m_{\mathrm{O}})}[n_O]$. Then, $\mathcal{O}$ can be defined as $(n_{\mathrm{O}} \pm \Delta_{\mathrm{r}}, m_{\mathrm{O}} \pm \Delta_{\mathrm{v}})$ to account for the object peak of some width in range Δ_{r} or velocity Δ_{v} .

Variable	Description
$S_{\mathrm{IF}}^{(m)}[n]$	value of RD map at row (fast-time) n, column (slow-time) m
n_{O}	fast-time index of object peak maximum
m_{O}	slow-time index of object peak maximum
N	number of fast-time samples
M	number of slow-time samples
$N_{\mathcal{O}}$	number of fast-time samples corresponding to object peak
$M_{\mathcal{O}}$	number of slow-time samples corresponding to object peak

Table 4.1: Description of variables used in (4.1) - (4.3).

Naturally, the ultimate measures for sensor performance are in fact the

- probability of detection $\mathrm{P_{de}}$ and
- probability of false alarm $\mathrm{P_{fa}}$.

These values highly depend on the object detection algorithm that is used. An extensive analysis is therefore difficult. Nevertheless, an object detection step is simulated and the probabilities computed for basic comparison.

For simplicity's sake, a single-object scenario is considered throughout the analysis of these measures. While different object signals can be generally considered independently due to the linearity of processing operations, an increase in the number of objects can have an effect on the performance of (some) mitigation methods. Such specific properties are investigated in addition to the framework of general performance comparison.

4.2 Simulation Results

4.2.1 Methodology

In Chapter 2, we introduced the parameters that affect the resulting interference of the RD map. Then in Chapter 3, the focus lied on the classification and general description of interference mitigation algorithms. A number of properties specific to certain algorithms have been mentioned. Finally in Section 4.1, performance assessment was addressed.

Considering this framework, the relation of "input" parameters (of victim, objects, interferers, as well as of the algorithms themselves) to "outputs" (metrics) is not trivial. The connections are too complex to analyze every possible parameter set individually. Therefore, there are two approaches to be used. First, a small number of example cases have been used throughout this work to pinpoint properties critical to mitigation processing. Second, to make general statements about algorithms, a Monte Carlo simulation is done.

A simulation run consists of a random choice of the number of interferers and their signaling parameters, akin to the ones listed in Table 2.1. Most parameters of the victim radar itself are kept fixed for simplicity. The parameters then correspond to a certain ramp scenario, such as the one depicted in Fig. 2.9. Input interference P_{int} and receiver noise (AWGN) powers P_{n} are set randomly, as well. The random choice of input signal parameters was done by drawing

from a uniform distribution. Tables 4.2 and 4.3 list the relevant parameters of the simulated victim radar system and interferers, respectively. Tables 4.4 and 4.5 are a summary of the tested methods and their parameters.

Parameter	Description	**Set Value**
$f_{0,\mathrm{V}}$	ramp start frequency	76GHz
B_{V}	ramp bandwidth	1GHz
T_{V}	ramp duration	48µs
B_{IF}	IF bandwidth	20MHz
N	number of fast-time samples	2048
N_{zp}	N after zero-padding	4096
M	number of slow-time samples	128
M_{zp}	M after zero-padding	256
window	type used	Hann

*Table 4.2: Simulated **victim** radar and signal processing parameters.*

Parameter	Description	**min.**	**max.**
# of interferers	-	1	3
$f_{0,\mathrm{I}}$	ramp start frequency	75.8GHz	76.2GHz
B_{I}	ramp bandwidth	0.6GHz	1.4GHz
T_{I}	ramp duration	40µs	46µs
P_{I}	transmit power	13dB	33dB
P_{N}	noise power	-20dB	-5dB

Table 4.3: Range of random interferer (and receiver noise) parameters.

Method	**Description**
zero	Zeroing, see Section 3.2
R-lip.	Linear Interpolation over Ramps (Slow Time Domain), see Section 3.3.1
RF	Ramp Filtering, see Section 3.5
RFPC	Ramp Filtering with added Phase Correction, see Section 3.5.1
TDSub	Time Domain Subtraction, see Section 3.4
IMAT	IMAT, see Section 3.6
IVMip	Time Domain Parametric Interpolation, see Section 3.3

Table 4.4: Summary of simulated methods.

Figure 4.1 depicts the CDFs of the resulting P_{int} and P_{n} over the simulations, respectively. The essential goal of this Monte Carlo simulation is to obtain results over a range of the relevant parameters. Practical interest is for the resulting amplitudes, forms, durations and locations of interference bursts to vary as much as possible, while also corresponding to realistic ramp scenarios.

In Fig. 4.2a , it can be seen that the simulation essentially corresponds to a sweep over the cases of none to all ramps being interfered. However, in Fig. 4.2b we observe that the total percentage of interfered samples is in a relatively smaller range, concentrated around $\approx 10\%$. This is inherently due to the nature of crossing ramp sequences. While ramps with similar slopes result in an interference burst of longer duration, such ramps also generally cross less often.

The different output metrics can be presented and analyzed *statistically*. In particular, the collected values of each metric can be observed as a *distribution*. This allows for a simple assessment of average performance and robustness, in terms of mean and spread of the distribution.

Method	Parameters
zero	no inverse window used
R-lip.	-
RF	filter operation: (global) minimum
RFPC	-
TDSub	-
IMAT	Δ , $\eta_{\max}$ computed adaptively as proposed in [38]
IVMip	$\eta = 2$, $\Delta = 16$, $N_{\text{est}} = 1024$

Table 4.5: Choice of algorithm-specific parameters for the different methods.

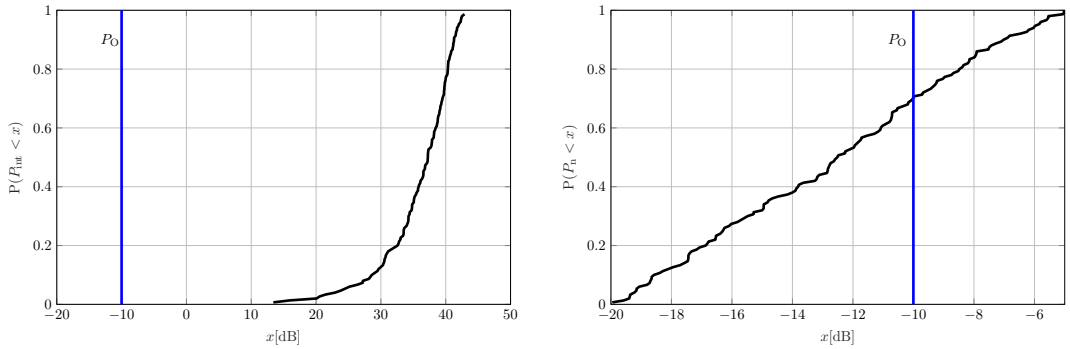

(a) Distribution of total interference power prior to processing.

(b) Distribution of receiver noise power prior to processing.

Figure 4.1: CDF (Cumulative Distribution Function)s of interference and receiver noise power. The constant object signal power level is added to the plot as $P_{\text{O}} = -10$dB as a reference. Note that power here is meant in the "sample energy" sense, such as in Eq. (2.21).

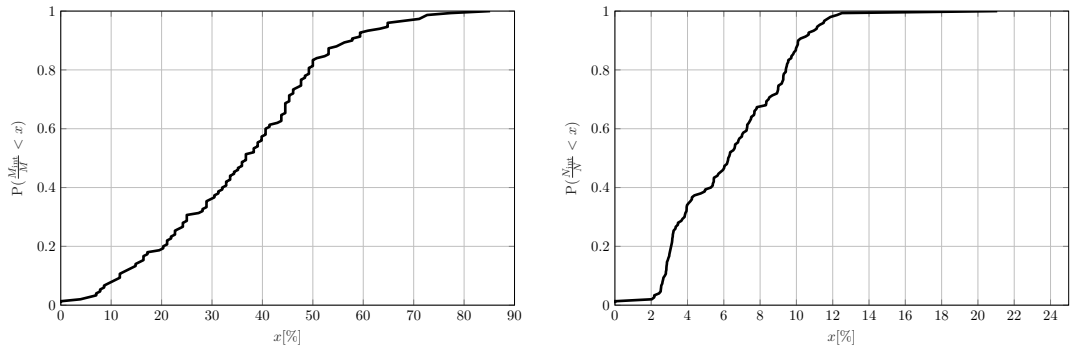

(a) Distribution of the percentage of interfered ramps.

(b) Distribution of the percentage of total interfered samples of the RD matrix.

Figure 4.2: Number of interfered ramps and samples resulting over the simulation runs, respectively.

Mitigation algorithm metrics are compared to the non-mitigated, the non-interference case and to each other in this way.

Another important point to consider is the effect of the AAF, as well as that of non-ideal detection of interfered samples. First, the idealized case for the form of an interference burst as considered initially (see, e.g., Fig. 2.1b), as well as perfect detection are discussed. The same results are presented then, when including a *9-th order Butterworth low-pass filter* and a basic *adaptive thresholding interference detection* into the simulation framework.

The coming sections are a summary of the results.

4.2.2 Gain in SINR due to Mitigation Processing

Figures 4.3 and 4.4 illustrate the noise suppression behavior of the algorithms in range and velocity domains, respectively.

- Without mitigation processing, the SINR is simply the consequence of the input powers (see Fig. 4.1) with the standard RD processing gains as described in Section 2.5. The distribution is very similar for both domains.
- Time domain subtraction offers the worst performance in terms of SINR gain out of the analyzed algorithms. As we have already seen (Fig. 3.5), due to estimation inaccuracies there is a significant remaining interference signal. The gain of this method appears to be approximately constant, with no significant change in the form of the distribution when compared to the "no mitigation" case.
- Simple zeroing offers superior performance to the previously mentioned subtraction method, since it guarantees a complete elimination of the interference component (although also that of a part of the object signal).
- Interpolation using IVM yields very similar performance to zeroing. This means that the estimation of the object frequency with the parameters used as listed in Table 4.5 is insufficiently accurate. Since the same false object signal model is used to interpolate over the interference bursts in every ramp, the performance even suffers from a degradation over zeroing in the velocity domain.
- The two non-parametric interpolation algorithms exhibit quite similar behaviors. Both of them are significantly more effective than the previously discussed techniques in this context. IMAT offers a slightly better performance in range. It is, however, less robust than linear ramp interpolation in velocity domain. This can be explained by ramp interpolation attempting to preserve the "continuity" of the time domain signals, while IMAT replaces bursts of interfered samples as a whole, possibly introducing phase uncertainty at the edges of the replaced burst. An option to alleviate said effect could be to use some method of smoothing at these edges.
- Ramp filtering, both with and without phase correction, yields the highest SINR in range domain. It can be observed that in fact the gain at the object range is even higher than in the case of a non-interfered clean object signal. This is possible due to the minimum operator, naturally setting the noise floor to its lowest value. As expected, in the velocity domain a significant performance degradation is visible if no phase correction is employed.

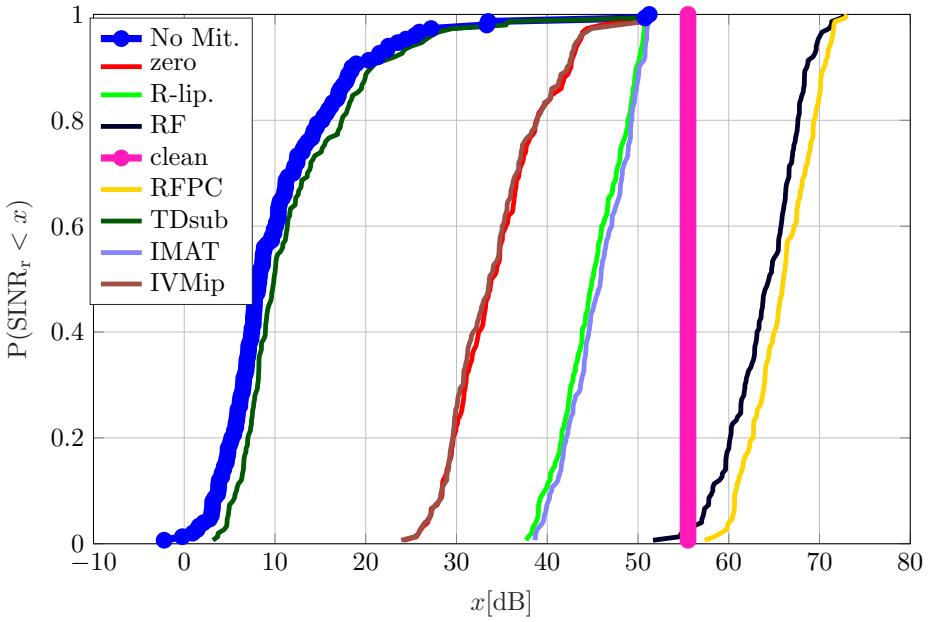

Figure 4.3: CDF of $\mathrm{SINR_r}$

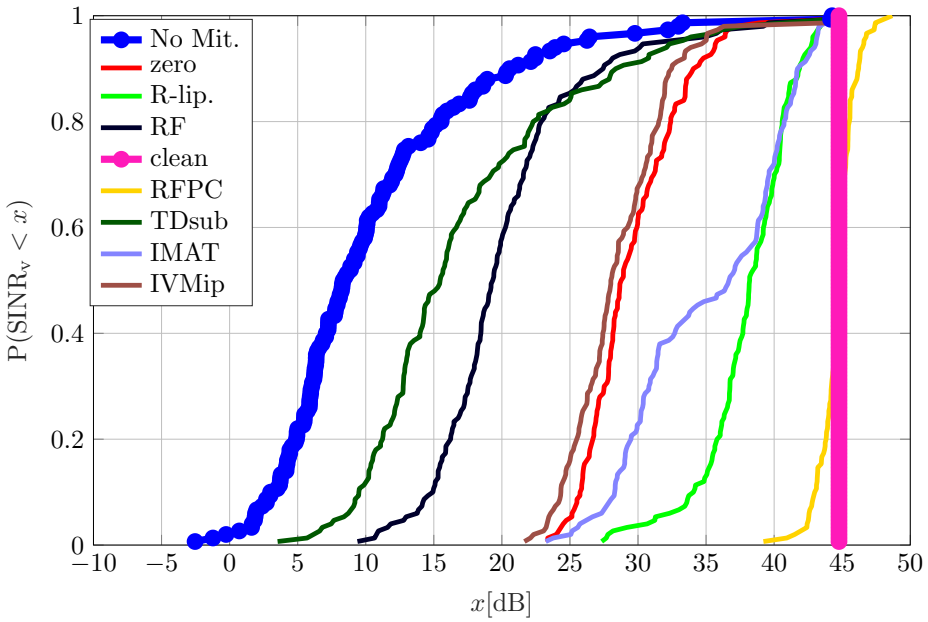

Figure 4.4: CDF of $\mathrm{SINR_v}$

Effect of Imperfect Interference Detection

In Figures 4.5 and 4.6, it can be seen that the performance of methods dependent on interference sample detection worsens considerably. In particular the performance gap between zeroing and the non-parametric interpolation techniques (IMAT, R-lip.) is decreased. The performance of Ramp Filtering is unaffected.

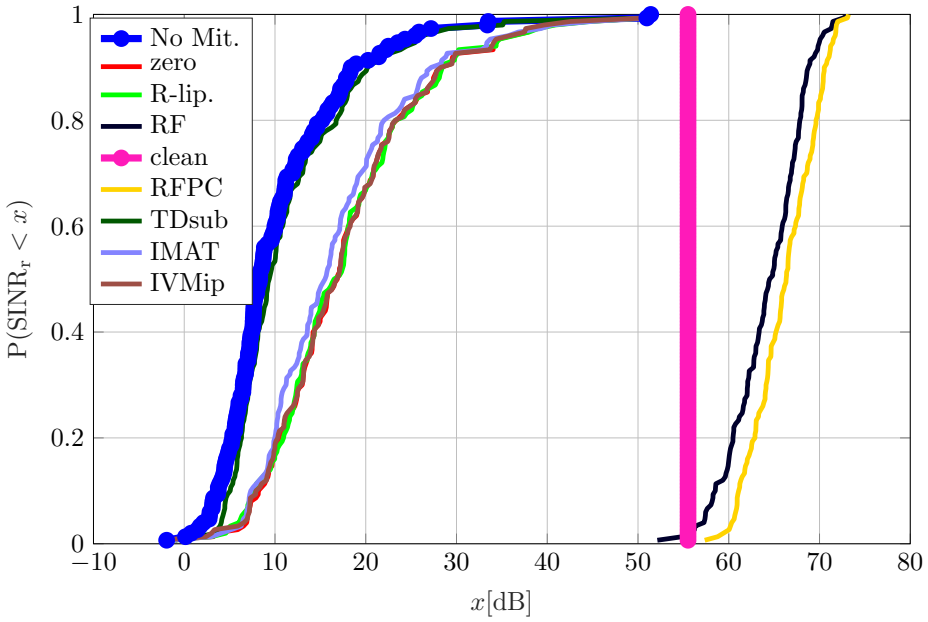

Figure 4.5: CDF of $\mathrm{SINR_r}$ *with non-ideal interference detection.*

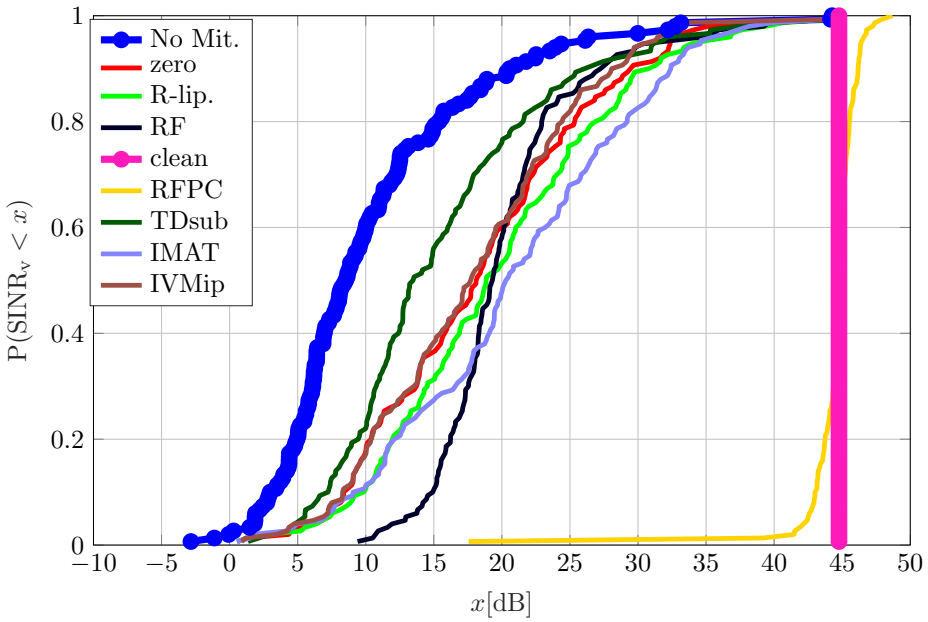

Figure 4.6: CDF of $\mathrm{SINR_v}$ *with non-ideal interference detection.*

4.2.3 Detection and False Alarm Probabilities

Over all the simulation runs, detections are compared to the simulated "ground truth" to compute a single detection and false alarm probability value, respectively. Fig. 4.7 is a visualization of the results.

Key points from Fig. 4.7a include the following.

- Every method leads to a drastic improvement in detection probability. This is intuitive, considering the SINR gains of the methods as seen in the previous section.
- Zeroing, and all methods implicitly based on it, work well because (as seen in Fig. 4.2b) the total number of interfered samples does not exceed $\approx 20\%$.

- Time domain subtraction exhibits the worst performance, since it only partially removes interference energy.

The main observations from Fig. 4.7b are as follows.

- A more diverse set of values can be observed for the false alarm probability.
- All methods except ramp filtering improve this metric when compared to the non-mitigated case.
- The two non-parametric interpolation techniques decrease the metric the most. This is due to their ability to increase the SINR while avoiding the introduction of artifacts on the RD map.
- Time domain subtraction and parametric interpolation yield worse results than zeroing. This can be explained by their respective behaviors, as already discussed in Section 4.2.2.
- Ramp filtering, both with and without additional phase correction, significantly increase the false alarm probability. The reason is that the algorithm selects a single sample of the noise floor, and copies it to every ramp before the computation of the second FFT. This means that the noise statistics of the RD map is altered, possibly leading to minor local peaks that can then be detected by a CFAR-type detector. While a relatively strong effect unique to ramp filtering, a slight modification of the algorithm or at the detector could probably solve this issue. Additionally, note that object detection is in fact already implicitly a part of the phase correction algorithm. In that case therefore, a reconstruction of the RD matrix and subsequent detection is not necessary.

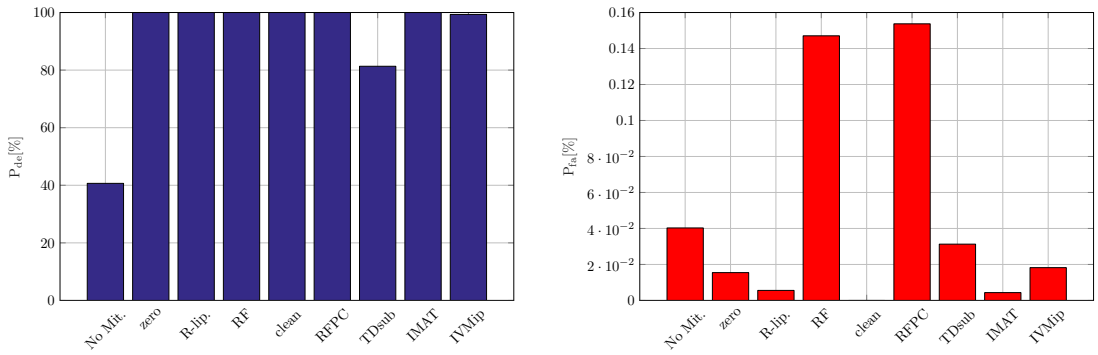

(a) Detection probabilities. *(b) False alarm probabilities.*

Figure 4.7: Illustration of the computed P_{de} *and* P_{de} *of the different methods.*

Effect of Imperfect Interference Detection

In Figure 4.8, we observe a bigger diversity of P_{de} values. The result matches well to that of the SINR values as presented on the previous plots. The two non-parametric interpolation techniques lead to a modest improvement over zeroing, while parametric interpolation appears to have no effect, due to reasons discussed before. The effectiveness of Ramp Filtering, as mentioned, remains unchanged.

It should be emphasized once more that the determination of detection and false alarm probability metrics was done using only a single, essentially arbitrarily parameterized CA CFAR detector. The results, while useful, are therefore not representative, since there are many possibilities of detector structure and parameters. An extensive discussion of detectors is out of the scope of this thesis and could be a part of future work.

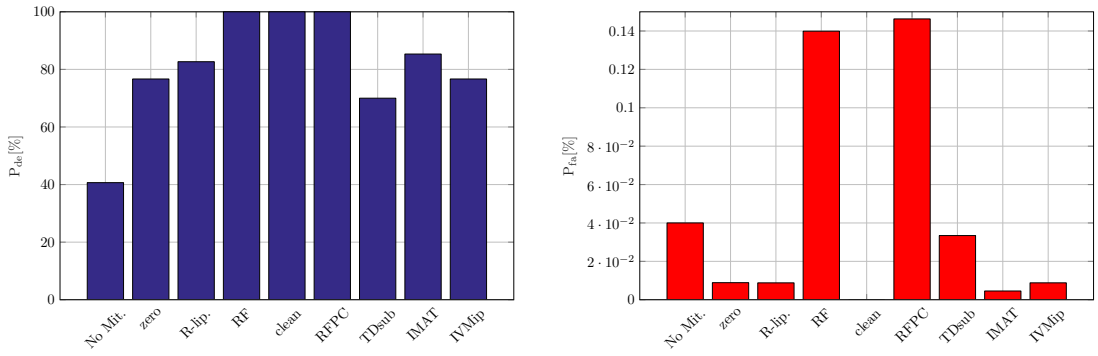

(a) Detection probabilities. *(b) False alarm probabilities.*

Figure 4.8: Illustration of the computed $\mathrm{P_{de}}$ *and* $\mathrm{P_{de}}$ *of the different methods for the non-ideal interference detection case.*

4.2.4 Value of the Detected Object peak

The EVM is computed according to (4.3) at the object sample index for every simulation run. The results are depicted in Fig. 4.9. The main points of analysis are the following.

- Ramp filtering distorts the object value the most. Such behavior is essentially a direct consequence of the non-linear approach of this method. Naturally, applying slow-time phase correction improves performance. Still, time domain methods in general seem to more easily maintain the original magnitude and initial phase value of the object signal. This is understandable, considering that said methods only alter part of the input samples prior to RD processing.
- Subtraction has a limited effect due to imperfect interference component deletion, consistent with previous observations of the other metrics.
- Zeroing introduces an error, also related to the loss of resolution (as illustrated in Fig. 3.2). Parametric interpolation does not improve on the performance of zeroing, again reinforcing the result that the estimated object model is in fact not acceptably accurate.
- Non-parametric interpolation techniques yield the best results.

Effect of Imperfect Interference Detection

Looking at Fig. 4.10, it can be noted that the advantage time domain algorithms had in repairing the object peak value essentially vanishes. Each method improves on the EVM metric over the non-mitigated case, but none of them seems significantly better than the others.

As mentioned previously, the actual value of the detected peak on the RD map is useful for subsequent signal processing. The magnitude might be used for clustering/classification of objects. More importantly, however, the phase value in particular is used for angle estimation when using several receive channels. For this, the *phase difference* of the detected peak value over the receive channels is evaluated.

Interference mitigation processing would generally be applied on every channel in a MIMO system. Hence, if the error introduced by the algorithm to the peak value is the same for all receive channels, it might not in fact lead to an erroneous angle estimate. Since in this work only single-channel simulations have been presented, such considerations are the subject of further research.

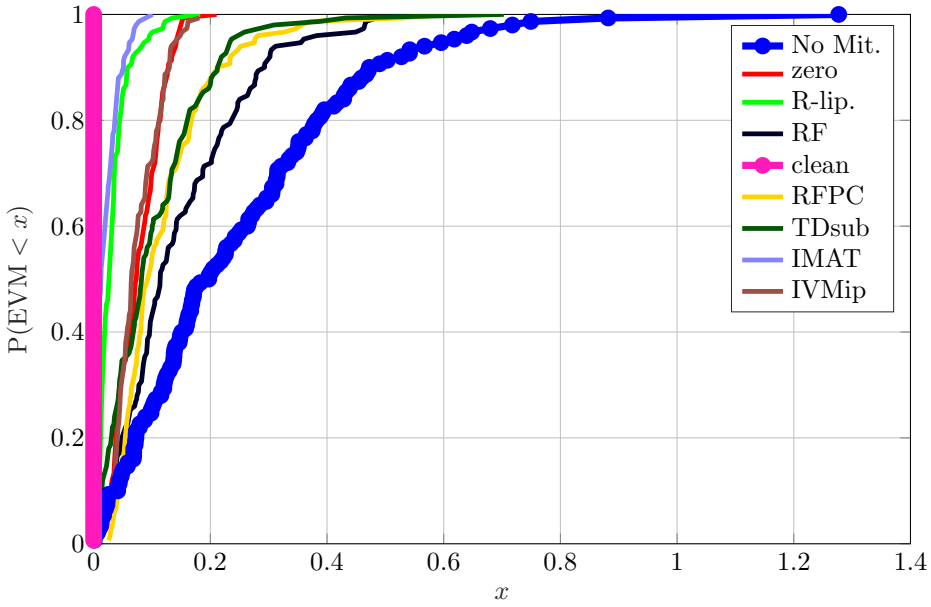

Figure 4.9: CDF of EVM

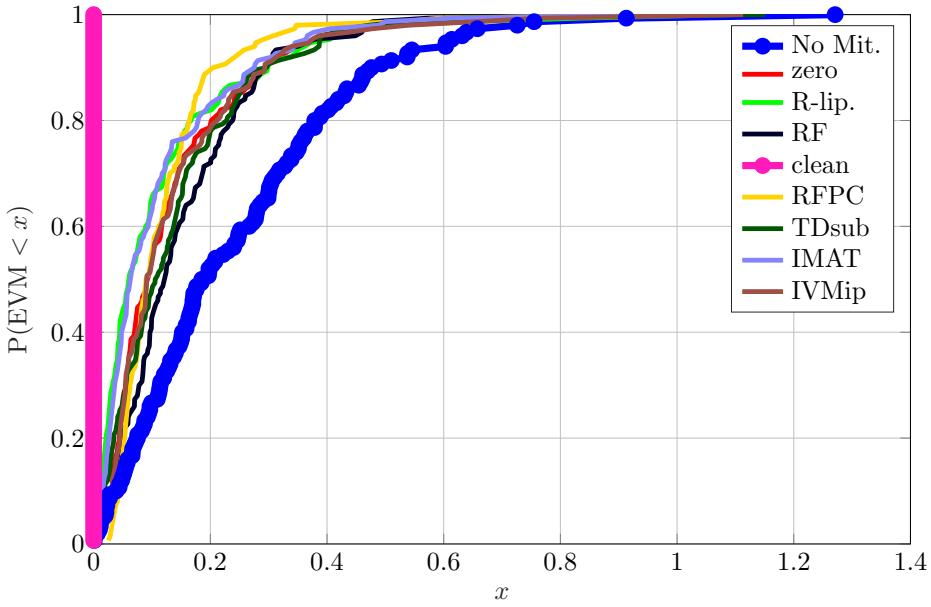

Figure 4.10: CDF of EVM for the non-ideal interference detection case.

4.3 Application of the Algorithms to Measurement Data

In Section 2.4, measurement data was compared with simulated signals in order to verify the analytical model described in this work. For a description of the conducted measurements, see Appendix A.1. In this section, a brief example of testing interference mitigation algorithms on measurement signals is presented.

The interference scenario used for this example is the one introduced in Section 2.4.2. In particular, the non-mitigated signal on Fig. 4.11 corresponds to the measurement signal of Fig. 2.15c. The effects of the different time domain techniques are visible. The interfered samples are detected the same way as in (the imperfect detection case of) last section.

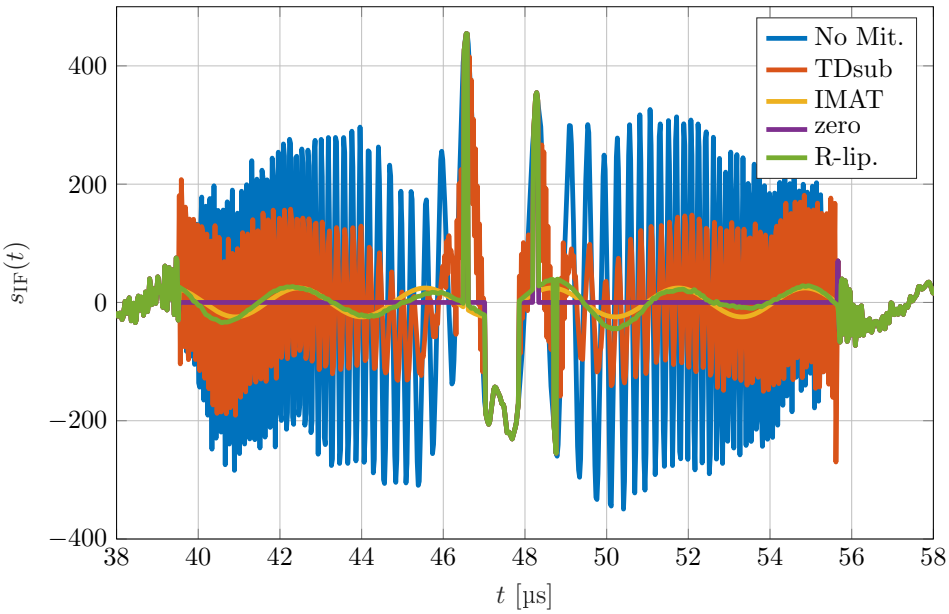

Figure 4.11: Plot of one of the interference bursts and the results of mitigation processing.

Since metrics cannot be computed explicitly here, performance on the RD map is visualized by range and velocity profiles. This is done at the maximum value in both dimensions of the RD matrix, termed $d_{\max}$ and $v_{\max}$, respectively. Depictions of the results can be inspected in Figures 4.12 and 4.13.

The scenario is static, meaning that each peak is concentrated at $v = 0$ on the velocity profile. In range domain, there are several peaks to be seen, close by each other as well as relatively close to the measurement sensor itself. These points are not surprising when considering the measurement scenario.

In terms of mitigation performance, effects are generally relatively subtle. This might be explained by the SINR in fact already being quite high without any additional processing, since the power output by the interfering sensor was not very high itself. However, the noise suppression performance of Ramp Filtering in particular is very apparent on the range profile.

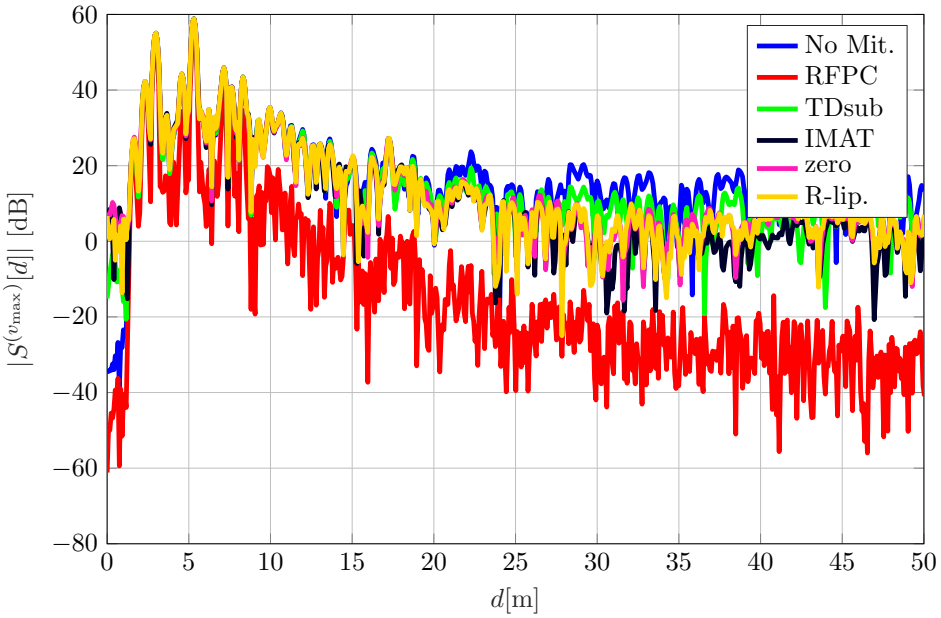

Figure 4.12: Range profile.

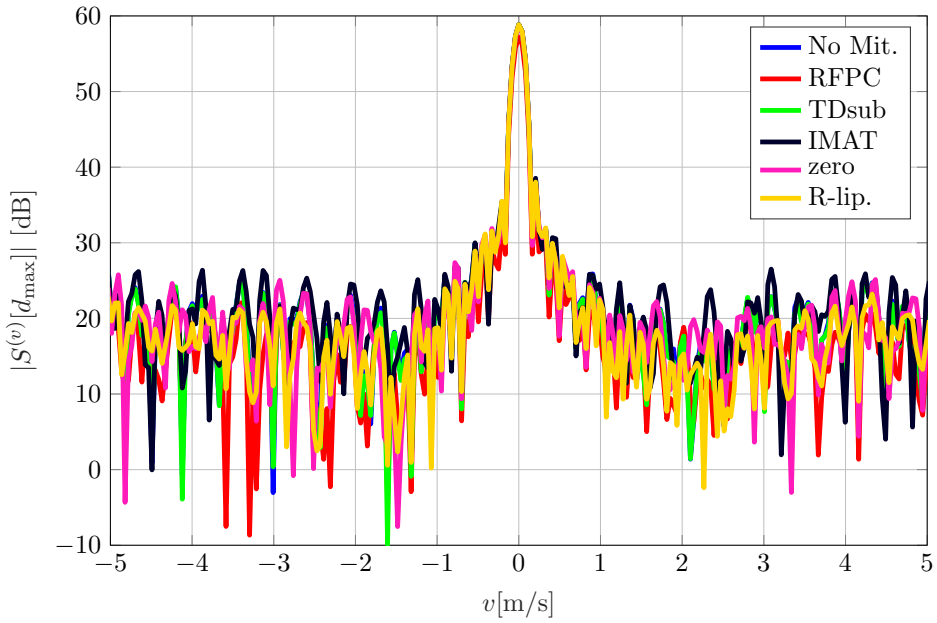

Figure 4.13: Velocity profile.

4.4 Summary and Conclusion of this Chapter

The key points from this chapter can be listed as:

- Parametric methods, in the forms used in this work, are not particularly effective. The reason is essentially the high accuracy requirements of the associated parametric estimation, as well as the issue of model legitimacy itself. More sophisticated algorithms might be needed, which however further increase computational complexity and might need further specific model assumptions.
- Non-parametric interpolation techniques show a promising performance with the advantage of low EVM.

- All time domain methods investigated in this chapter are, however, highly dependent on accurate interfered sample detection.
- Ramp Filtering possesses the highest SINR in range domain, as well as in velocity domain, but only if phase correction is used. In addition, it is the only method not directly needing, and hence robust against, interference detection errors. Issues concerning EVM and P_{fa} arise, and should be investigated further.

5 Conclusion and Outlook

5.1 Conclusion

In this work a partial answer is given to the question: *"How does mutual interference affect FMCW radar and how to mitigate possibly significant detrimental effects?"* However, this general issue entails several aspects and has been addressed in different ways in the past already. Existing results consisted of estimates for *interference probability* and *average received interference power*, as well as proposals of several methods for interference mitigation, among others.

This thesis presents an *exact model* of non-coherent interference. First, a time domain model is established based on parameters pertaining to a single interference burst. The frequency spectrum is then derived analytically. In the case of a symmetric, real-valued time domain signal, it can be observed that the spectral magnitude is modulated by a chirp and the spectral phase is linear. The main insight is that the form of the interference spectrum differs significantly from spectral whiteness, and in certain cases can be described relatively simply. While this suggests the potential effectiveness of parametric interference mitigation methods, it is pointed out that the signal form is extremely sensitive to parameter changes, leading to very high requirements on parameter estimation accuracy.

The notion of *ramp-coherence* is introduced for the *statistical description* of the effects of interference on the RD map. In the ramp-incoherent case, the effect of interference on the RD map can be approximated by AWGN. In contrast, ramp-coherent interference leads to the interference energy concentrated at certain regions on the RD map. This reinforces that interference can possibly lead to vastly different outcomes for different scenarios. The importance of robust interference mitigation algorithms is highlighted thereby.

Furthermore, a *comparative analysis* of several state of the art interference mitigation methods is performed. It is confirmed that the analyzed parametric methods do not perform as well as non-parametric techniques. Time domain interpolation methods are shown to cause the least distortion of the object signal due to mitigation processing, but depend highly on the detection of interfered samples. The approach of ramp filtering shows very promising SINR gain, however, it alters the value of object signal and the form of the RD map. The fundamental strengths and weaknesses of each algorithm are shown in this way. The usefulness of the introduced *performance metrics* is proven through these findings.

The specific research questions posed in Section 1.1.3 can be answered in the following way.

- It *is possible* to systematically investigate interference, combining parametric signal modeling with statistical considerations. Generalizing the resulting framework to account for every possibility in practice is certainly a challenge, however.
- Based on an understanding of the underlying signal models, we are able to statistically analyze a limited number of extracted general performance measures. Statements about the *performance* and *robustness* of mitigation methods can therefore be made. Methods can be ranked according to the measures, confirming the methods' respective properties. Declaring a single best algorithm remains difficult, though.

Ultimately, it is becoming increasingly clear that interference mitigation needs to be considered as an integral part of the future automotive radar signal processing chain. The framework introduced in this thesis aims to facilitate the systematic development of suitable mitigation methods in the future.

5.2 Ongoing and Further Work

Following this thesis, there remain a large number of highly interesting and relevant questions considering the topic that could be addressed in further research.

In particular, further signal processing steps not dealt with in this work are to be considered. A treatise on the detection of interfered samples for time domain methods would be useful. A more thorough investigation of object detection algorithms could be performed, to explore their interplay with interference mitigation processing. MIMO processing should be included into the signal model, as well, as an additional potential dimension of mitigation.

Furthermore (while estimates and simulation results as mentioned already exist in the literature), it is still ultimately unclear how frequent and severe different kinds of interferences will actually be on the roads in the future. Addressing this issue would be a significant part of model development, ideally leading to a scalable, practical and accurate view on interference. Methods of statistical traffic and environment modeling need to be employed therefore, to be then ultimately combined with signal-level models such as the ones presented in this thesis. The above task would also entail conducting measurements in more realistic environments.

In the context of realistic modeling, there might exist relevant properties of actual sensor hardware that have been insufficiently addressed in previous analyses. Effects arising due to the large signal dynamics of high-power interference, e.g. amplifier non-linearities, possibly have a significant influence on the signal model. Hence, more research in this area is also needed.

It is to be mentioned that the development of new mitigation methods is continuously ongoing. The list of techniques treated in this thesis certainly does not exhaust the possibilities.

Finally, signaling schemes other than FMCW and their mutual interference could be further investigated. Interference robustness might become an important aspect in the development of future radar technologies.

A Appendix

A.1 Brief Description of Measurement Setup

Qualitative measurements to demonstrate interference have been conducted as part of this work. Two identical *INRAS RadarLog* boards were used as measurement hardware, acting as victim and interfering sensor, respectively. The connected front-end includes 4TX and 16RX channels operating in the 77GHz band. For an exact description of the hardware, see [54]. The most important hardware-specific settings for the measurement are summarized in Table A.1. An example of the signaling parameters set for a measurement has been given in Table 2.2.

Table A.1: Relevant receiver settings and properties.

Parameter	**Value / Description**
ADC sampling frequency	40 MHz
IF bandwidth	20 MHz
AAF cut-off frequency	14 MHz ; exact type unknown
analog high-pass filter	exact type unknown

Figure A.1: Photograph of the measurement scene.

Figure A.1 is a photograph taken of the measurement location. It is a medium-sized, indoors conference room. The sensors are placed on a table in front of each other, with two corner reflectors places on the same table, as well. While unfortunately no exact ground truth is available, the locations of these objects were determined by a rough measurement, see Table A.2.

The received IF signals are saved to a file which is then post-processed in MATLAB. In Fig. A.2, 16 receive channels were used for MIMO processing, yielding a two-dimensional map

*Table A.2: Locations of the sensors and reflectors in a two-dimensional coordinate system with dimensions **x** and **y**.*

	x	**y**
victim	0	0
interferer	0	1.7m
reflector (small)	-0.7m	2.3m
reflector	0.8m	3.1m

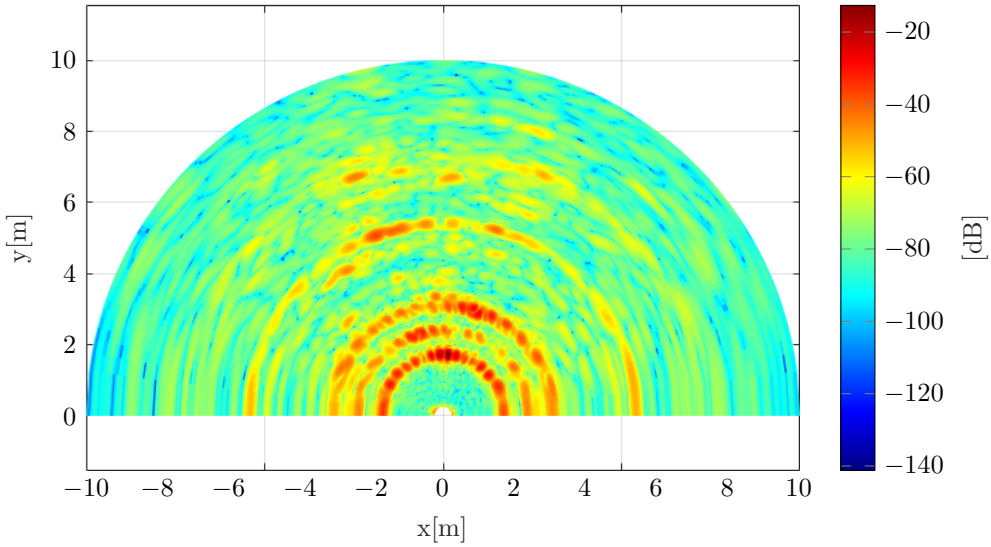

Figure A.2: Result of distance and angle measurement, depicted in two-dimensional coordinates. The interferer was inactive for this example.

of the sensed environment. The interfering sensor was disabled and therefore only acts as an object itself. While peaks at the locations described in Table A.2 can be recognized, we can observe a large number of different reflections. This is due to the cluttered office environment, which is not ideal for radar measurements. Interference measurements in more controllable as well as realistic environments are to be done in the future.

Bibliography

[1] H. Meinel and J. Dickmann, "Automotive Radar: From Its Origin to Future Directions," *Microwave Journal*, vol. vol.56, pp. 24–40, 09 2013.

[2] J. Dickmann, J. Klappstein, M. Hahn, N. Appenrodt, H. L. Bloecher, K. Werber, and A. Sailer, "Automotive radar the key technology for autonomous driving: From detection and ranging to environmental understanding," in *2016 IEEE Radar Conference (RadarConf)*, May 2016, pp. 1–6.

[3] M. Kunert, H. Meinel, C. Fischer, and M. Ahrholdt, "Report on interference density increase by market penetration forecast," the MOSARIM Consortium, Tech. Rep. D16.1, Sep. 2010.

[4] S. M. Patole, M. Torlak, D. Wang, and M. Ali, "Automotive radars: A review of signal processing techniques," *IEEE Signal Processing Magazine*, vol. 34, no. 2, pp. 22–35, Mar. 2017.

[5] R. F. Tigrek, W. J. A. de Heij, and P. van Genderen, "Multi-carrier radar waveform schemes for range and Doppler processing," in *2009 IEEE Radar Conference*, May 2009, pp. 1–5.

[6] H. Haderer, R. Feger, C. Pfeffer, and A. Stelzer, "Millimeter-wave phase-coded cw mimo radar using zero- and low-correlation-zone sequence sets," *IEEE Transactions on Microwave Theory and Techniques*, vol. 64, no. 12, pp. 4312–4323, Dec 2016.

[7] A. G. Stove, "Linear FMCW radar techniques," *IEE Proceedings F - Radar and Signal Processing*, vol. 139, no. 5, pp. 343–350, Oct 1992.

[8] H. Rohling and M. M. Meinecke, "Waveform design principles for automotive radar systems," in *2001 CIE International Conference on Radar Proceedings (Cat No.01TH8559)*, 2001, pp. 1–4.

[9] V. Winkler, "Range Doppler detection for automotive FMCW radars," in *2007 European Microwave Conference*, Oct 2007, pp. 1445–1448.

[10] D. Göhring, M. Wang, M. Schnürmacher, and T. Ganjineh, "Radar/Lidar sensor fusion for car-following on highways," in *The 5th International Conference on Automation, Robotics and Applications*, Dec 2011, pp. 407–412.

[11] J. Bechter, C. Sippel, and C. Waldschmidt, "Bats-inspired frequency hopping for mitigation of interference between automotive radars," *2016 IEEE MTT-S Int. Conf. Microwaves Intell. Mobility, ICMIM 2016*, no. 1, 2016.

[12] G. M. Brooker, "Mutual Interference of Millimeter-Wave Radar Systems," *IEEE Transactions on Electromagnetic Compatibility*, vol. 49, no. 1, pp. 170–181, Feb. 2007.

[13] M. Hischke, "Collision warning radar interference," *IEEE Intell. Veh. Symp.*, pp. 13–18, 1995.

[14] B. E. Tullsson, "Topics in FMCW radar disturbance suppression," in *Radar 97 (Conf. Publ. No. 449)*, no. 449, 1997, pp. 1–5.

[15] M. Goppelt, H. L. Blöcher, and W. Menzel, "Analytical investigation of mutual interference between automotive FMCW radar sensors," in *2011 German Microwave Conference*, Mar. 2011, pp. 1–4.

[16] M. Goppelt, H.-L. Blöcher, and W. Menzel, "Automotive radar-investigation of mutual interference mechanisms," *Advances in Radio Science: ARS*, vol. 8, p. 55, 2010.

[17] A. Bourdoux, K. Parashar, and M. Bauduin, "Phenomenology of mutual interference of FMCW and PMCW automotive radars," in *2017 IEEE Radar Conference (RadarConf)*, May 2017, pp. 1709–1714.

[18] T. Schipper, T. Mahler, M. Harter, L. Reichardt, and T. Zwick, "An Estimation of the Operating Range for Frequency Modulated Radars in the Presence of Interference," *Proc. 10th Eur. Radar Conf.*, pp. 227–230, 2013.

[19] T. Schipper, *Modellbasierte Analyse des Interferenzverhaltens von Kfz-Radaren.* KIT Scientific Publishing, 2016, in German.

[20] C. Fischer, "Untersuchungen zum Interferenzverhalten automobiler Radarsensorik," Ph.D. dissertation, Universität Ulm, 2016, in German.

[21] C. Fischer, M. Barjenbruch, H. L. Bloecher, and W. Menzel, "Detection of pedestrians in road environments with mutual interference," in *2013 14th International Radar Symposium (IRS)*, vol. 2, June 2013, pp. 746–751.

[22] K. Hahmann, S. Schneider, and T. Zwick, "Evaluation of probability of interference-related ghost targets in automotive radars," in *ICMIM*, 2018, pp. 158–161.

[23] A. Al-Hourani, R. J. Evans, S. Kandeepan, B. Moran, and H. Eltom, "Stochastic Geometry Methods for Modeling Automotive Radar Interference," *IEEE Trans. Intell. Transp. Syst.*, pp. 1–11, 2017.

[24] T. Schipper, M. Harter, L. Zwirello, T. Mahler, and T. Zwick, "Systematic approach to investigate and counteract interference-effects in automotive radars," *Proc. 9th Eur. Radar Conf.*, pp. 190–193, 2012. [Online]. Available: http://services.lib.mtu.edu:2188/document/6450736/?arnumber=6450736{%}5Cnhttp://services.lib.mtu.edu:2188/ielx5/6423297/6450609/06450736.pdf?tp={&}arnumber=6450736{&}isnumber=6450609

[25] T. Schipper, S. Prophet, L. Zwirello, M. Harter, L. Reichardt, and T. Zwick, "Simulation framework for the estimation of future interference situations between automotive radars," *IEEE Antennas Propag. Soc. AP-S Int. Symp.*, pp. 2103–2104, 2013.

[26] T. Schipper, S. Prophet, M. Harter, L. Zwirello, and T. Zwick, "Simulative Prediction of the Interference Potential Between Radars in Common Road Scenarios," *IEEE Trans. Electromagn. Compat.*, vol. 57, no. 3, pp. 322–328, 2015.

[27] T. Schipper, J. Schlichenmaier, D. Ahbe, T. Mahler, J. Kowalewski, and T. Zwick, "A simulator for multi-user automotive radar scenarios," *2015 IEEE MTT-S Int. Conf. Microwaves Intell. Mobility, ICMIM 2015*, pp. 1–4, 2015.

[28] F. Torres, C. Frank, W. Weidmann, T. Mahler, T. Schipper, T. Zwick, and M. Kunert, "The Norm-Interferer - an universal tool to validate 24 and 77 GHz band automotive radars," *Radar Conf. (EuRAD), 2012 9th Eur.*, pp. 9–12, 2012.

[29] M. Kunert, "The EU project MOSARIM: A general overview of project objectives and conducted work," in *2012 9th European Radar Conference*, Oct 2012, pp. 1–5.

[30] ——, "Study report on relevant scenarios and applications and requirements specification," the MOSARIM Consortium, Tech. Rep. D12.1, 2010.

[31] M. Kunert and C. Fischer, "Use cases description list for simulation scenarios," the MOSARIM Consortium, Tech. Rep. D3.1, 2011.

[32] M. Kunert, H. Meinel, C. Fischer, and M. Ahrholdt, "GENERATION OF AN INTERFERENCE SUSCEPTIBILITY MODEL," the MOSARIM Consortium, Tech. Rep. D2.2, 2011.

[33] M. Kunert, "Study on the state-of-the-art interference mitigation techniques," the MOSARIM Consortium, Tech. Rep. D1.4, 2010.

[34] C. Fischer, H. L. Blöcher, J. Dickmann, and W. Menzel, "Robust detection and mitigation of mutual interference in automotive radar," in *2015 16th International Radar Symposium (IRS)*, June 2015, pp. 143–148.

[35] M. Barjenbruch, D. Kellner, K. Dietmayer, J. Klappstein, and J. Dickmann, "A method for interference cancellation in automotive radar," *2015 IEEE MTT-S Int. Conf. Microwaves Intell. Mobility, ICMIM 2015*, 2015.

[36] J. Bechter and C. Waldschmidt, "Automotive radar interference mitigation by reconstruction and cancellation of interference component," in *2015 IEEE MTT-S Int. Conf. Microwaves Intell. Mobility, ICMIM 2015*, 2015, pp. 0–3.

[37] J. Bechter, K. D. Biswas, and C. Waldschmidt, "Estimation and cancellation of interferences in automotive radar signals," in *2017 18th International Radar Symposium (IRS)*, Jun. 2017, pp. 1–10.

[38] J. Bechter, F. Roos, M. Rahman, and C. Waldschmidt, "Automotive Radar Interference Mitigation Using a Sparse Sampling Approach," in *Proc. 14th Eur. Radar Conf.*, 2017, pp. 90–93.

[39] M. Wagner, F. Sulejmani, A. Melzer, P. Meissner, and M. Huemer, "Threshold-Free Interference Cancellation Method for Automotive FMCW Radar Systems," in *Proc. IEEE International Symposium on Circuits and Systems (ISCAS 2018)*, May 2018, accepted for publication.

[40] J. Bechter, K. Eid, F. Roos, and C. Waldschmidt, "Digital beamforming to mitigate automotive radar interference," *2016 IEEE MTT-S Int. Conf. Microwaves Intell. Mobility, ICMIM 2016*, pp. 2–5, 2016.

[41] J. Bechter, M. Rameez, and C. Waldschmidt, "Analytical and experimental investigations on mitigation of interference in a DBF MIMO radar," *IEEE Trans. Microw. Theory Tech.*, vol. 65, no. 5, pp. 1727–1734, 2017.

[42] Y. Kim, "Identification of FMCW radar in mutual interference environments using frequency ramp modulation," *2016 10th Eur. Conf. Antennas Propagation, EuCAP 2016*, 2016.

[43] M. A. Hossain, I. Elshafiey, and A. Al-Sanie, "Mutual interference mitigation in automotive radars under realistic road environments," in *2017 8th International Conference on Information Technology (ICIT)*, May 2017, pp. 895–900.

[44] M. Toth, P. Meissner, A. Melzer, and K. Witrisal, "Analytical Investigation of Non-Coherent Mutual FMCW Radar Interference," in *Proc. European Radar Conference (EuRAD 2018)*, Sep. 2018, accepted for publication.

[45] C. Cook and M. Bernfeld, *Radar Signals: An Introduction to Theory and Application*, ser. Electrical Science, H. G. Booker and N. DeClaris, Eds. Academic Press, 1967.

[46] M. Abramowitz and I. A. Stegun, Eds., *Handbook of Mathematical Functions With Formulas, Graphs and Mathematical Tables*, ser. Applied Mathematics. National Bureau of Standards, 1964, vol. 55.

[47] M. Richards, *Fundamentals of Radar Signal Processing*, ser. Professional Engineering. McGraw-Hill Education, 2005. [Online]. Available: https://books.google.at/books?id=j91oJ22ldoQC

[48] Y. Chan, J. Lavoie, and J. Plant, "A Parameter Estimation Approach to Estimation of Frequencies of Sinusoids," *IEEE Trans. Acoust.*, vol. ASSP-28, no. 2, pp. 214–219, 1981.

[49] W. Greene, *Econometric Analysis*. Pearson Education, 2003. [Online]. Available: https://books.google.at/books?id=njAcXDlR5U8C

[50] S. Kay, *Fundamentals of Statistical Signal Processing: Estimation Theory*. Prentice-Hall PTR, 2013. [Online]. Available: https://books.google.at/books?id=JaSctQEACAAJ

[51] F. Marvasti, M. Azghani, P. Imani, P. Pakrouh, S. Heydari, A. Golmohammadi, A. Kazerouni, and M. Khalili, "Sparse signal processing using iterative method with adaptive thresholding (IMAT)," in *2012 19th International Conference on Telecommunications (ICT)*, April 2012, pp. 1–6.

[52] A. Golyandina, N. and Zhigljavsky, *Singular Spectrum Analysis for Time Series*. Springer Berlin Heidelberg, 2013, vol. 1.

[53] M. Ghil, M. R. Allen, M. D. Dettinger, K. Ide, D. Kondrashov, M. E. Mann, A. W. Robertson, A. Saunders, Y. Tian, F. Varadi, and P. Yiou, "ADVANCED SPECTRAL METHODS FOR CLIMATIC TIME SERIES," *Rev. Geophys.*, vol. 40, no. 1, pp. 1–41, 2002.

[54] A. Haderer, "Radarlog User Manual," 2016. [Online]. Available: http://www.inras.at/produkte/new-radarlog.html